INVESTIGATION OF ULTRASTRUCTURAL AND MECHANICAL PROPERTIES OF RAT CORTICAL BONE USING MICRO-CT, THREE-POINT BENDING TESTING, AND THE REFERENCE POINT INDENTATION TECHNIQUE

BY

JOHN A. JAST

THESIS

Submitted in partial fulfillment of the requirements
for the degree of Master of Science in Mechanical Engineering
in the Graduate College of the
University of Illinois at Urbana-Champaign, 2011

Urbana, Illinois

Advisor:

Professor Iwona M. Jasiuk

ABSTRACT

Characterization of bone is important as it aids in the understanding of bone pathologies and their corresponding treatments. Assessment of cortical bone morphology has been identified as an important aspect of overall bone quality as it contributes significantly to the mechanical strength of bone. In the first part of this study, rat cortical bone was assessed at different hierarchical levels using micro-CT imaging, and changes within the cortical network morphology as a function of age were investigated. Decomposition of the intracortical porosity of the rat into the canal network and the osteocyte lacunar system allowed for the quantification of morphometric indices describing the size, shape, and spatial orientation of these systems. The porosity due to canals decreases with age while the porosity due to lacunae decreases slightly with age. Overall, it was found that the lacunae element-based parameters were independent of age. The results of this study serve as valuable inputs into the computational modeling of bone at different hierarchical scales and will help provide new insights into the assessment of bone quality in the future.

In addition to micro-CT imaging, the mechanical properties of rat cortical bone as a function of age were assessed with three-point bending testing. Additionally, a novel microindentation technique, termed reference point indentation (RPI),that is capable of *in vivo* testing was used to assess the mechanical properties of rat bone. These results were compared to traditional bending test results for validation of this new RPI technique. Parameters including apparent modulus, stiffness, mean energy dissipation, and ultimate bending strength were reported. Furthermore, a parameter unique to the RPI technique, the indentation distance increase (IDI), was introduced and used to investigate the fracture properties of bone as a function of age. It was concluded that the RPI technique is capable of providing information regarding bone fracture toughness as well as other parameters, and these parameters were similar to those obtained using traditional three-point bending tests. Although these results are promising, a more thorough comparison of the RPI technique with traditional mechanical testing is warranted to provide a better understanding of the relationship between these testing methods.

ACKNOWLEDGEMENTS

I would first like to extend my sincere gratitude and appreciation to Dr. Iwona M. Jasiuk for her help and guidance throughout my undergraduate and graduate studies. Her insight has greatly helped me accomplish many of my goals throughout my academic career. Additionally, I would like to thank Alexander Proctor and Kevin Bebak for their help with the BioDent™ instrumentation and data analysis. I would also like to thank Dr. Liang Feng for all his teaching and training; I could not have accomplished all I have without his help. Finally, I would like to sincerely thank my wife Kelsey and son Declan for all their patience, love, and support throughout the past few years.

TABLE OF CONTENTS

CHAPTER 1: INVESTIGATION OF ULTRASTRUCTURAL PROPERTIES OF RAT CORTICAL BONE USING MICRO-CT

1.1 INTRODUCTION

Cortical bone is a dynamic, living tissue that has a complex and continuously evolving microstructure that changes throughout life. Assessment of cortical bone morphology has been identified as an important aspect of overall bone quality (Schneider *et al.*, 2007) as it contributes significantly to the mechanical strength of bone (Mazess, 1990). A vital component of cortical bone microstructure is the canal network, an interconnected system of canals that perforate cortical bone and facilitate the distribution of vascular structures throughout the cortex (Marotti *et al.*, 1980). The structure of this cortical canal network changes as bone develops in order to promote vascularization and blood perfusion and ensure the supply of adequate oxygen, minerals, and nutrients necessary for bone strength and integrity (Brookes *et al.*, 1998; Brandi *et al.*, 2006). Therefore, it is necessary to investigate the morphometric properties of the canal network in growing bone as this may shed light on multiple areas of bone biology and elucidate the physiological significance of canalization within cortical bone. The three-dimensional analysis of the canal network may provide information regarding cortical bone structural dynamics at this level (Cooper *et al.*, 2007b).

Until recently, the analysis of cortical bone microstructure and the canal network has largely been restricted to two-dimensional histomorphometry or three-dimensional image registration of two-dimensional serial sections (Stout *et al.*, 1999; Parfitt *et al.*, 1983). Although beneficial, these techniques are time-consuming and ultimately result in destruction of the specimen (Alkemper *et al.*, 2001). Serial section preparation in particular is tedious and subject to deformation artifacts. Additionally, these techniques cannot provide a complete visualization of the three-dimensional microstructure of cortical bone.

Micro-computed tomography (micro-CT) has come into use for the three-dimensional analysis of bone structure *in vitro*, as first introduced by Feldcamp and colleagues (Feldcamp *et al.*, 1989). Micro-CT offers several advantages including the ability to non-destructively provide

quantitative results with little to no sample preparation. Although the technique has quickly become the standard for quantification and visualization of the three-dimensional structure of trabecular bone, its application to analysis of the internal microstructures within cortical bone has been more limited. Much work has been done using desktop micro-CT to analyze cortical bone porosity (Wachter *et al.,* 2001; Cooper *et al.,* 2003; Basillais *et al.,* 2007). However, much less has been done applying this technology to the assessment of the cortical microstructure of small rodents. Due to the smaller scale of the vascular canal network of these animals, analysis of rat and mouse cortical bone has been only been achieved through the use of synchrotron radiation micro-CT (SRμCT) (Matsumoto *et al.,* 2006; Matsumoto *et al.,* 2007; Schneider *et al.,* 2007). The use of SRμCT offers many advantages over conventional desktop micro-CT imaging including higher spatial resolution and the elimination of beam-hardening artifacts (Bonse *et al.,* 1996; Dilmanian, 1992), allowing for the determination of local bone mineralization (Nuzzo *et al.,* 2002; Sone *et al.,* 2004). However, access to SRμCT is often very limited, so it is desirable to obtain higher resolution images with desktop micro-CT imaging.

In this study, the rat was chosen for investigation because rat models are frequently used to assess bone structural and mechanical variations due to many factors including diet (Jiang *et al.,* 1997), physical activity (Umemura *et al.,* 1997; Kannus *et al.,* 1996), and disease (Han *et al.,* 1998; Jamsa *et al.,* 2002). Aging is a natural process that also alters bone properties and is therefore the interest of many studies. Britz *et. al.* demonstrated the possibility of visualization and quantification of the cortical microstructure of the rat using a desktop micro-CT system (Britz *et al.,* 2010), but an investigation of how this microstructure changes with age has not yet been conducted. Thus, the primary purpose of this study was to visualize and quantify changes in the cortical microstructure of the rat as a function of age.

As outlined by Schneider *et al.* (Schneider *et al.,* 2007), cortical bone tissue was assessed following a hierarchical approach, beginning at the macroscopic (organ) level and proceeding down to the sub-microscopic (cellular) level. In addition to the determination of various indices at each level, an effort was made to subdivide the total intracortical porosity and identify the contributions of each the canal network and the osteocyte lacunar system to overall porosity. In

addition, the spatial orientation of osteocyte lacunae within the canal network was investigated. Investigation of the ultrastructural morphology of bone at different hierarchical scales can provide valuable information regarding the evaluation of bone quality and the modeling of bone at these scales.

1.2 MATERIALS AND METHODS

1.2.1 TISSUE PREPARATION

Tibiae were excised from female Sprague-Dawley rats obtained from control rats of previous studies. The rats ranged from infant to adult and included ages of 3 weeks (n=5), 12 weeks (n=5), 32 weeks (n=5), 42 weeks (n=5), 60 weeks (n=5), and 72 weeks (n=5). The background of each previous study was considered to ensure that its proceedings had no effect on the factors investigated in the current study. After harvesting and soft tissue removal, the bones were wrapped in gauze and soaked in a 0.1M phosphate buffered saline solution to prevent dehydration. The samples were then stored at -20°C in sealed freezer bags.

1.2.2 BONE HIERARCHICAL STRUCTURE

For purposes of this study, bone was modeled as a hierarchical structure, characterized by various structures at different length scales. Within this study, three of these levels are considered. At the macrostructural level, cortical bone is characterized by its volume distribution and radial growth and is considered to be compact. The canal network constitutes the microstructural level and is considered a part of the ultrastructure of the intracortical porosity. Also a part of this ultrastructure, the osteocyte lacunar system is described in the sub-microstructural level due to its smaller size and variant morphology.

1.2.3 MICRO-CT IMAGING

Macrostructure - Whole Bone

In accordance with the convention set forth by Kuhn *et al.* (Kuhn *et al.*, 1990), micro-CT images will herein be referred to as slices, and ground bone fragments will be referred to as

sections. Additionally, micro-CT imaging guidelines, nomenclature, and reported parameter selection were adapted from a comprehensive review paper by Bouxsein and colleagues (Bouxsein *et al.*, 2010). For imaging at the macrostructural scale (1-50cm), a scan of the whole tibia bone was conducted. The tibiae were thawed to 4°C in a refrigerator for 24 hours prior to imaging. During scanning, samples were kept wrapped in saline-soaked gauze and enclosed in plastic eppindorf tubes. These tubes were mounted on a platform using double sided adhesive carbon tape to prevent sample drift over time. The samples were scanned using a SkyScan 1172 (Aartselaar, Belgium) X-ray microtomograph. The samples were rotated 360 degrees at a rotation step of 0.7 degrees. The X-ray settings were standardized to 60 kV and 160 μA, and two-frame averaging was utilized to improve the signal-to-noise ratio. Total scanning time for each sample was approximately 3 hours, and a nominal resolution of 12 μm was achieved. To create a set of contiguous transverse cross-sectional slices from the acquired angular projections, the volumetric reconstruction software Nrecon 1.4 was used (SkyScan software). The reconstruction process included beam-hardening correction, alignment optimization, and ring artifact reduction.

Microstructure

Following imaging of the whole bone, the tibiae were sectioned to prepare samples suitable for imaging at the microstructural scale (10-500 μm). Tibiae were cut into transverse sections with a thickness of 400 μm using an Isomet 1000 precision diamond saw (Buehler, Lake Bluff, IL), and the subsample sections were taken from the mid-diaphyseal region of the tibiae. These sections of bone were then immediately submerged in a fixative of 2.0% paraformaldehyde and 2.5% glutaraldehyde in 0.1M Na-Cacodylate buffer for 4 hours at 4°C. Following fixation, the sections were subjected to a buffer rinse of 0.1M Na-Cacodylate for 10 minutes. The sections were then progressively dehydrated at room temperature in 37%, 67%, and 95% ethanol, each for 10 minutes and finally in 100% ethanol for 30 minutes (solution change every 10 minutes). Once dehydrated, the sections were supercritically dried using a Samdri-PVT-3D Critical Point Dryer (Tousimis, Rockville, MD, USA) to prevent drying artifacts and sample damage due to surface tension. The samples were scanned using an Xradia

MicroXCT-200 (Pleasanton, CA) to obtain a 4.0 μm resolution. The X-ray settings were standardized to 40kV and 200 μA. A total of 500 slices were obtained, corresponding to a stack height of 2mm in length along the mid-diaphysis.

Sub-microstructure

Following sectioning using a slow speed saw, the remaining portions of tibiae were prepared for imaging at the sub-microstructural scale (1-10μm) and the visualization of the osteocyte lacunar network. The proximal half of each tibia was rinsed with 100% ethanol twice (10 minutes each) at room temperature and then left in 100% ethanol at 4°C for 24 hours. After infiltration with methacrylate monomer, the samples were embedded in polymethyl methacrylate (PMMA) and sectioned into 150 μm thick slices using a Leica RM2255 rotary microtome (Leica Microsystem Inc, Bannockburn, IL) with a tungsten carbide blade. Under a microscope, the extra plastic was trimmed away from around the bone specimen using a razor blade. The samples were scanned using an Xradia MicroXCT-400 (Pleasanton, CA) to obtain a 1.0 μm resolution. X-ray settings were standardized to 50kV and 200 μA, and exposure time per frame was 8 seconds.

1.2.4 IMAGE POST-PROCESSING

The micro-CT data sets were analyzed using Amira 5.3.0 (Visage Imaging Inc, San Diego, CA). The images were translated from 16bit grayscale images (0-65535) into 8bit grayscale images (0-255), and void space comprised of the canal network and osteocyte lacunae were identified using a standardized global threshold. The Amira Quantification+ software addition option was used to conduct quantitative analysis including automated segmentation, extraction of geometrical information, and filtering.

Quantitative Morphometry

Morphometric indices assessed in this study were adapted from those utilized by Schneider et al. (Schneider *et al.*, 2007). Namely, at the macrostrutural level, total tissue volume

(TV) comprised of cortical bone and the medullary cavity, cortical bone volume (Ct.BV), cortical bone volume density (Ct.BV/TV), cortical thickness (Ct.Th), and polar area moment of inertia (J) were calculated.

At the microstructural level, indices similar to the cannular parameters introduced by Cooper *et al.* (Cooper *et al.*, 2003) and adapted from three-dimensional trabecular bone analysis (Hildebrand *et al.*, 1999) were used for quantification of the canal network. The number of canals (N.Ca), cortical total volume (Ct.TV) (including both cortical bone volume and void space), number density of canals (N.Ca/Ct.TV), total canal volume (Ct.V), and volume density of canals (Ca.V/Ct.TV) were calculated. In addition to parameters describing the canal network as a whole, the network was broken down into single elements and analyzed using element-based morphometry, similar to that utilized previously for the analysis of trabecular bone (Stauber *et al.*, 2006). In agreement with the nomenclature introduced by Schneider and colleagues (Schneider *et al.*, 2007), these element-based indices are average values calculated over the total number of elements and are designated by brackets (<>). These average values calculated include mean canal diameter (<Ca.Dm>), mean canal length (<Ca.Le>), mean canal orientation (<Ca.θ>) measured from the longitudinal axis of the tibia, and mean canal volume (<Ca.V>). An illustration of how mean canal length, diameter, and orientation were defined is given in Figure 1B. In addition to a global analysis of these parameters for the entire mid-diaphyseal region of the tibia, the canal indices were also computed separately for the four main anatomical sites (anterior, posterior, medial, lateral) to determine the dependence (if any) of these parameters on anatomical site. These quadrant divisions were determined by marking the axes at 45° to the anterior-posterior and medial-lateral axes on the transverse section of each sample (Figure 1A).

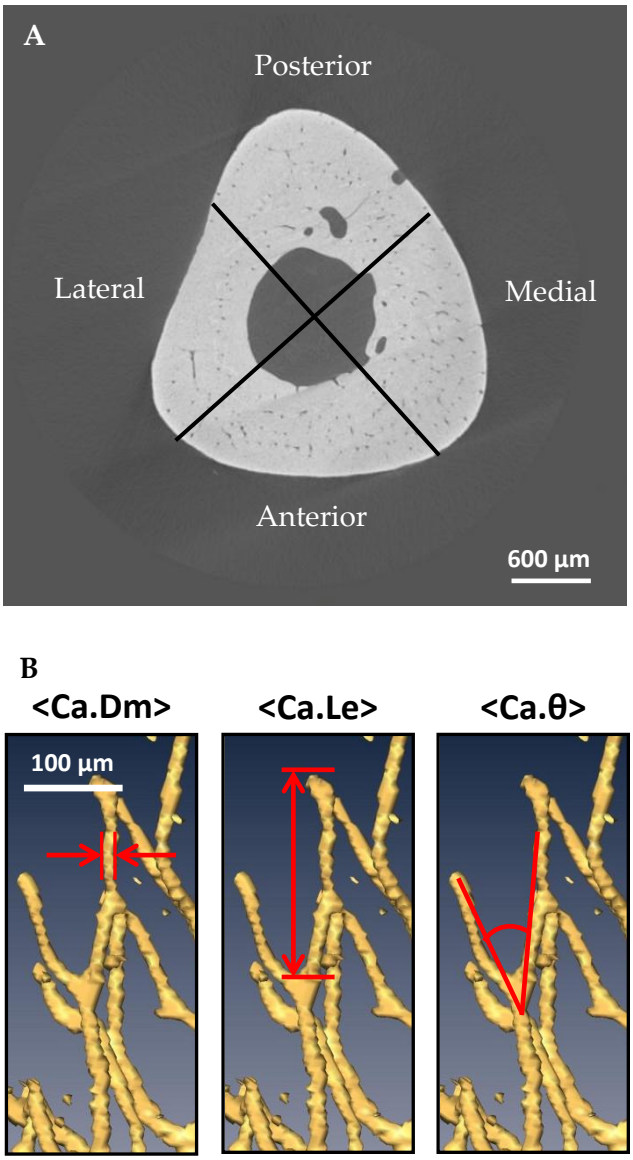

Figure 1. (A) Reconstructed image of a 12 week tibial transverse section. The image was divided into four sections for regional analysis. (B) Illustration of the canal network parameters used for quantitative assessment of the cannular network. From left to right, mean canal diameter (<Ca.Dm>), mean canal length (<Ca.Le>), and mean canal orientation (<Ca.θ>) are defined.

At the sub-microstructural level, similar to the negative imprint formed by the canal network, there exists the osteocyte lacunar system. Analogous to the analysis of the canal network, this cellular network was quantified using the following indices: lacuna number density (N.Lc/Ct.TV) and lacuna volume density (Lc.V/Ct.TV). Element-based indices were also calculated and include mean lacuna volume (<Lc.V>), mean lacuna length (<Lc.Le>), and mean lacuna orientation (<Lc.θ>) (measured from the longitudinal axis of the tibia).

1.2.5 STATISTICAL ANALYSIS

Statistical analysis was performed using OriginPro 8.1 (OriginLab Corp. Northampton, MA). The software was used to conduct one-way analysis of variance (ANOVA) to test for differences in mean parameter values between age groups. Additionally, Tukey's honestly significant difference (HSD) tests were performed as a post hoc analysis for pairwise comparisons among means to explicitly determine which parameters were significantly different from one another.

1.3 RESULTS

Morphometry results for the macrostructural level are summarized in Table 1. ANOVA revealed the existence of statistically significant differences between all indices among the various age groups, with $p < 0.001$ for each case. Tukey tests were performed as a post hoc analysis and revealed that the 3 week samples exhibited statistically significant differences in all indices compared to the rest of the age groups. Among samples of 12 weeks of age and older, there existed no significant differences in mean total tissue volume, mean cortical bone volume, mean cortical bone volume density, or mean cortical thickness ($p > 0.05$ for all cases). However, mean polar area moment of inertia values were statistically different between all age groups excepting 12, 32, and 42 weeks, which displayed no significant differences at the 0.05 level.

Table 1: Morphometric results at the whole bone level. Values are mean ± SD.

Parameter	3 week	12 week	32 week	42 week	60 week	72 week	ANOVA
TV (mm^3)	3.79 ± 0.43	7.52 ± 0.94	7.34 ± 0.82	6.48 ± 0.88	6.78 ± 1.11	6.81 ± 1.04	<0.001
Ct.BV (mm^3)	2.21 ± 0.5	6.32 ± 1.15	5.97 ± 1.09	5.56 ± 0.71	5.62 ± 0.8	5.39 ± 0.96	<0.001
Ct.BV/TV (%)	58.3 ± 5.5	84.1 ± 7.4	81.3 ± 7.2	85.7 ± 4.6	83 ± 6.2	79.1 ± 4.9	<0.001
Ct.Th (μm)	184 ± 36	676 ± 70	632 ± 55	642 ± 71	640 ± 53	622 ± 76	<0.001
J (mm^4)	0.13 ± 0.03	2.02 ± 0.18	2.5 ± 0.20	2.25 ± 0.23	3.42 ± 0.41	3.03 ± 0.29	<0.001

Morphometric results for the canal network at the microstructural level are tabulated in Table 2. ANOVA revealed that all indices except mean canal length displayed a statistically significant difference among the age groups. Specifically, there was a statistically significant ($p < 0.05$) increase in mean canal number density between 3 week samples and 12 week samples.

After 12 weeks of age, mean canal number density displayed a gradual decrease from 163 mm^{-3} to 128mm^{-3} at 72 weeks of age. Canal volume density is a measure of the contribution of the canal microstructures to the overall bone tissue porosity. There was a statistically significant increase ($p < 0.05$) in mean canal volume density between the ages of 3 and 12 weeks followed by a gradual decrease into 72 weeks of age. Mean canal volume displays a significant drop ($p < 0.05$) from $742 \cdot 10^3$ μm^3 at 3 weeks of age $426 \cdot 10^3$ μm^3 at 12 weeks before steadily decreasing eventually dropping to $339 \cdot 10^3$ μm^3 at 72 weeks. Mean canal diameter drops significantly from 29.7 μm at 3 weeks to 21.1 μm at 12 weeks, after which point the mean canal diameter remains relatively constant. While no significant variations were found between mean canal lengths for the age groups, there was a dependence of mean canal orientation on age ($p < 0.05$). Therefore, although the average length of individual canals does not change significantly with age, the spatial arrangement of this canal network and its branches does.

Table 2: Morphometric results at the microstructural level. Values are mean ± SD.

Parameter	3 week	12 week	32 week	42 week	60 week	72 week	ANOVA
N.Ca/Ct.TV (mm^{-3})	83 ± 10.8	163 ± 34.4	159 ± 28.7	139 ± 25	132 ± 22.3	128 ± 27.6	<0.001
Ca.V/Ct.TV (%)	6.13 ± 0.7	2.72 ± 0.6	2.53 ± 0.8	2.10 ± 0.9	1.71 ± 0.4	1.69 ± 0.6	<0.001
<Ca.V> ($10^3 \cdot \mu m^3$)	742 ± 131	426 ± 99	393 ± 87	345 ± 123	360 ± 108	339 ± 127	<0.001
<Ca.Dm> (μm)	29.7 ± 6.7	21.1 ± 4.1	18.9 ± 5.2	19.7 ± 4.7	20.3 ± 4.9	19.2 ± 4.4	0.022
<Ca.Le> (μm)	268 ± 31	305 ± 22	299 ± 15	287 ± 23	279 ± 18	280 ± 17	0.114
<Ca.θ> (deg)	31.2 ± 15	53.3 ± 13	57.9 ± 10	65.4 ± 11	63.1 ± 8	68.8 ± 8	<0.001

Table 3 displays the morphometric analysis for the osteocyte lacunar system. At this sub-microstructural level, ANOVA revealed that there exists no statistically significant difference in lacuna number density or lacuna volume density. Furthermore, all lacunae element-based parameters displayed no dependence on age ($p > 0.05$ for all parameters). For all ages, mean lacuna volume was approximately 290 μm^3 and mean lacuna length was approximately 18 μm. The osteocyte lacunae were mostly plate-like structures and ellipsoidal in shape, oriented mainly along the longitudinal axis of the tibia.

Table 3: Morphometric results at the sub-microstructural level. Values are mean ± SD.

Parameter	3 week	12 week	32 week	42 week	60 week	72 week	ANOVA
N.Lc/Ct.TV (mm^{-3})	46833 ± 5752	39073 ± 3412	43530 ± 3897	40793 ± 4198	42212 ± 3337	38955 ± 3470	0.056
<Lc.V> (μm^3)	294 ± 21	309 ± 30	286 ± 27	281 ± 26	288 ± 28	299 ± 31	0.641
Lc.V/Ct.TV (%)	1.37 ± 0.3	1.21 ± 0.4	1.24 ± 0.3	1.15 ± 0.3	1.22 ± 0.4	1.16 ± 0.3	0.921
<Lc.Le> (μm)	16.4 ± 3.9	17.6 ± 2.9	18.3 ± 3.8	17.7 ± 3.0	18.9 ± 3.6	16.6 ± 3.1	0.845
<Lc.θ> (deg)	15.1 ± 4.7	13.3 ± 5.6	12.3 ± 5.8	13.1 ± 2.4	12.5 ± 3.1	14.4 ± 3.0	0.894

In addition to the global assessment of age-related changes, the cannular indices calculated at the microstructural level were also calculated separately for each of the anatomical sites (anterior, posterior, medial, lateral) as illustrated in Figures 2 – 7. Figure 2 illustrates the age- and site-related changes in canal number density. Initially, from 3 - 32 weeks of age, there existed significantly less canals per volume of bone in the medial region of the tibia ($p < 0.05$). This effect became less pronounced in the 42 week samples and eventually disappeared at older ages. At 72 weeks, canal number density was significantly lower ($p < 0.05$) in the posterior and lateral regions.

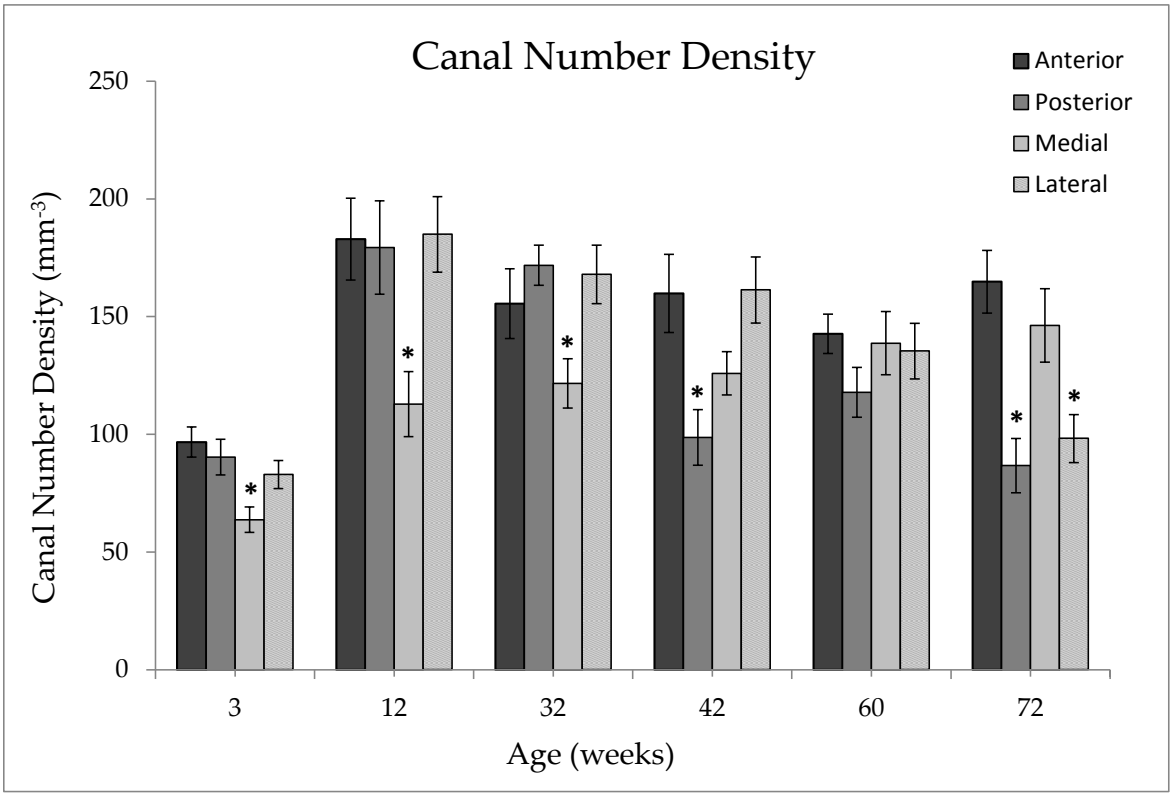

Figure 2. Age-related changes in canal number density at different anatomic sites. *denotes values statistically significantly different ($p < 0.05$) from another site according to Tukey's HSD test.

Figure 3 illustrates the age-related changes in canal volume density along with differences among various sites. At 3 weeks of age, the medial region contained significantly less porosity due to canals ($p < 0.05$) as compared to the other regions. This effect was seen throughout the 12 and 32 week samples, although this difference was not statistically significant. After 32 weeks, as age increased, the posterior region contained less porosity due to canals as compared to the other sites, and this effect was significant ($p < 0.05$) at 42 and 72 weeks of age. Similar to the trend displayed with canal number density within the 72 week samples, the canal volume density was also statistically significantly lower in the lateral region in the 72 week samples.

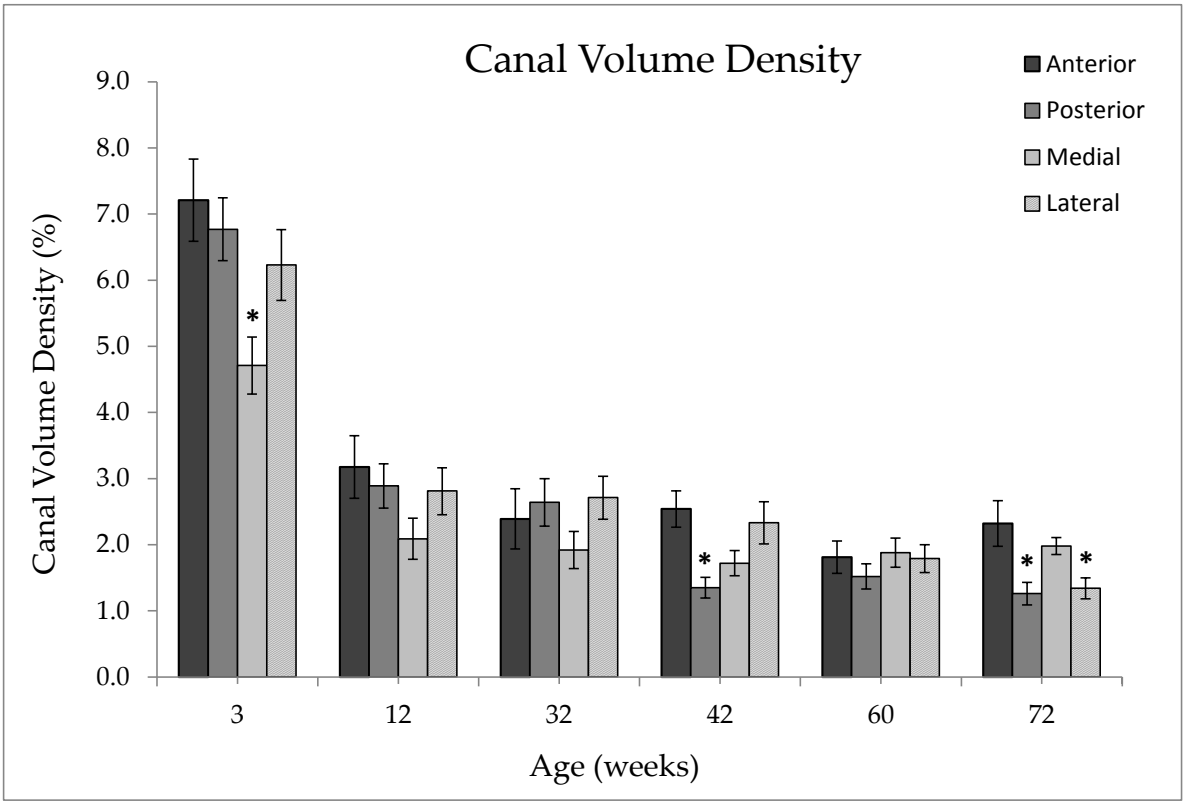

Figure 3. Age-related changes in canal volume density at various anatomical sites. *denotes values statistically significantly different ($p < 0.05$) from another site according to Tukey's HSD test.

Figures 4-7 illustrate the changes in element-based parameters with age and differences between anatomical sites. As shown in Figure 4, although there were changes with age, there was no statistically significant difference in mean canal volume between the anterior, posterior, medial, and lateral regions of the tibia. In fact, there was very close agreement between mean

canal volume measurements between the various sites at each age. As shown in Figure 5, mean canal diameter was also independent of anatomical location. Although there was less agreement between mean canal diameter measurements at each site, there were no significant differences between mean values ($p < 0.05$).

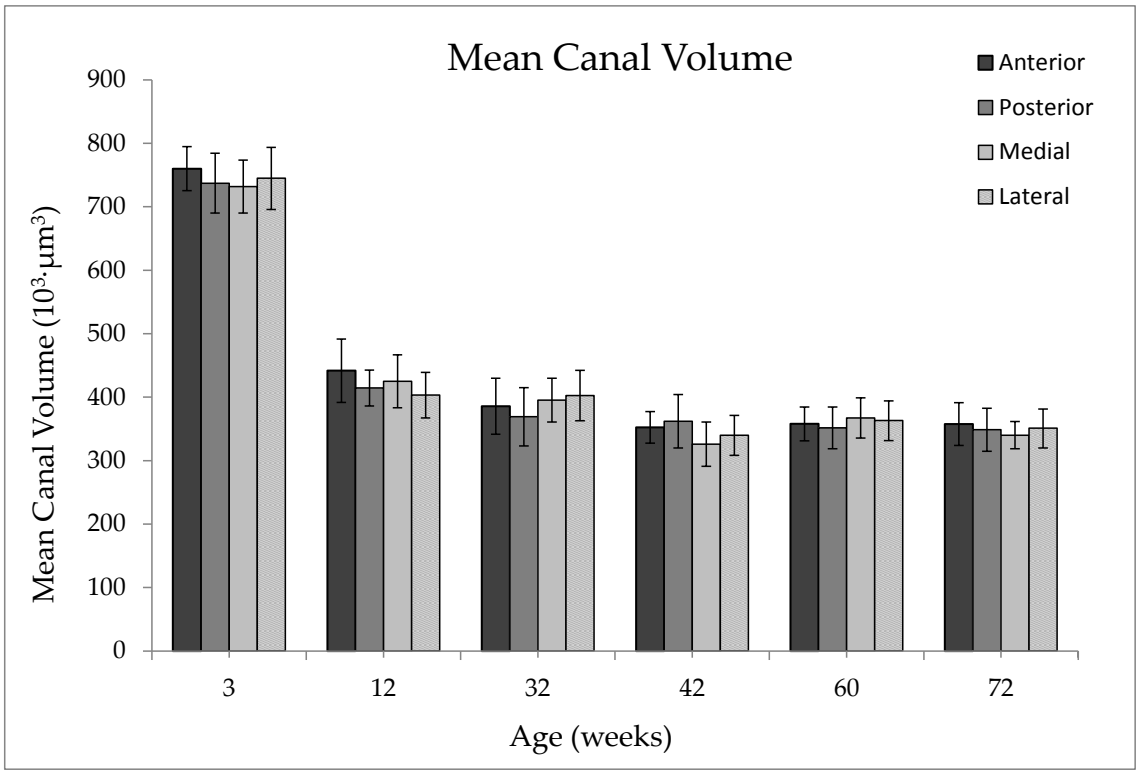

Figure 4. Age-related changes in mean canal volume at various anatomical sites.

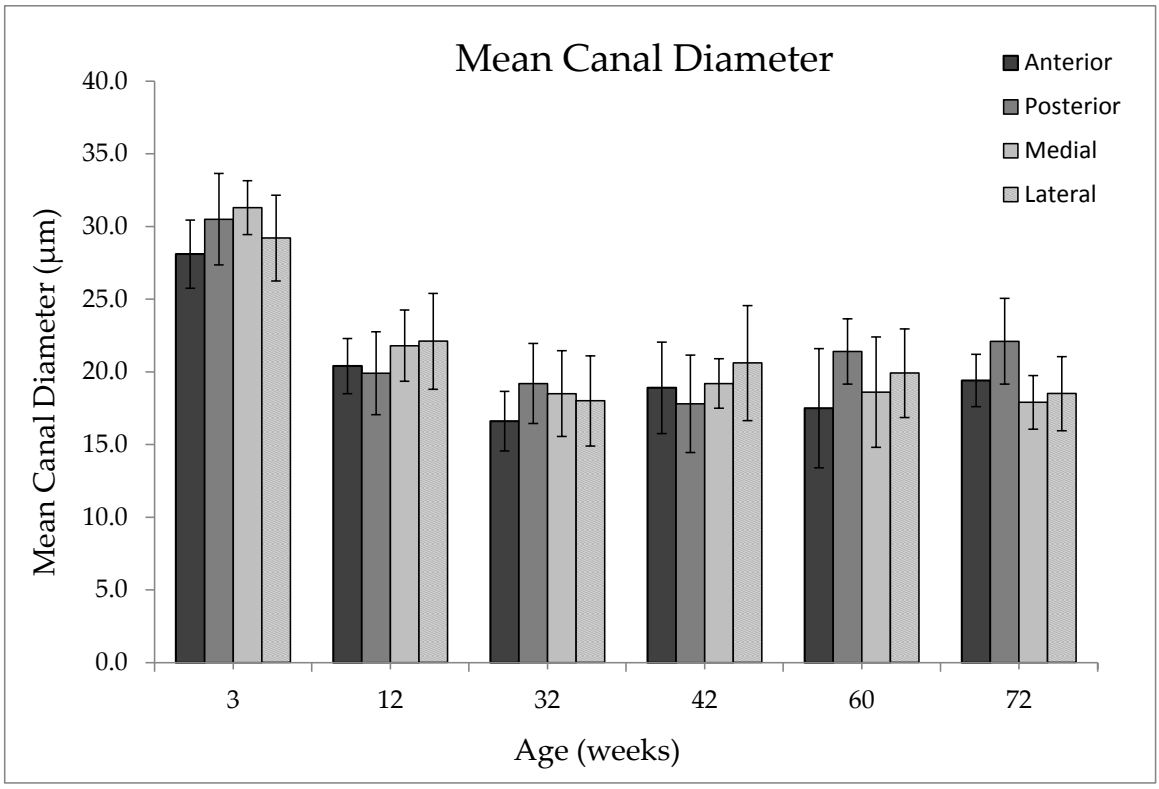

Figure 5. Age-related changes in mean canal diameter at various anatomical sites.

Figure 6 illustrates differences in mean canal length as a function of age and anatomical location. Although no statistically significant differences existed ($p > 0.05$ for all sites), there was a large decrease in mean canal length in the posterior region of the 72 week samples. Differences in mean canal orientation based on anatomical location are illustrated in Figure 7. At older ages (42, 60, and 72 weeks), the posterior region of the tibia exhibited canals with mean orientations that were greater (more radially-oriented) than other sites. This difference in mean canal orientation in the posterior region was statistically significant at 60 and 72 weeks of age ($p < 0.05$).

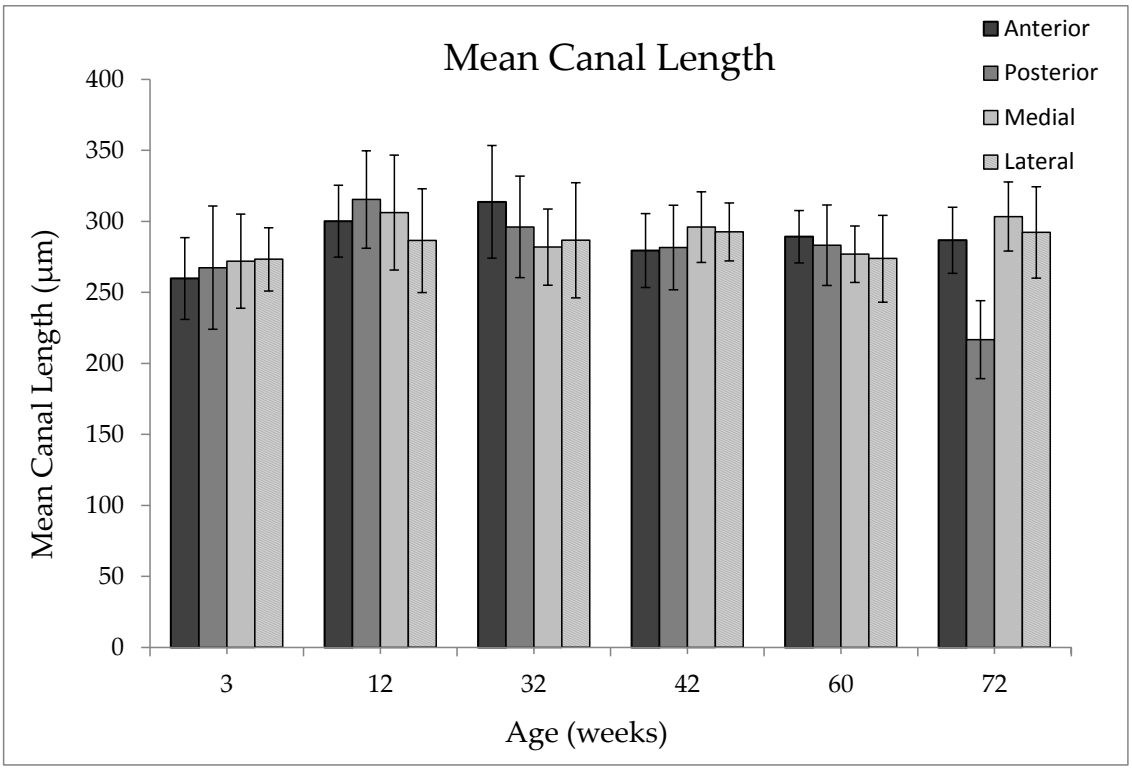

Figure 6. Age-related changes in mean canal length at various anatomical sites.

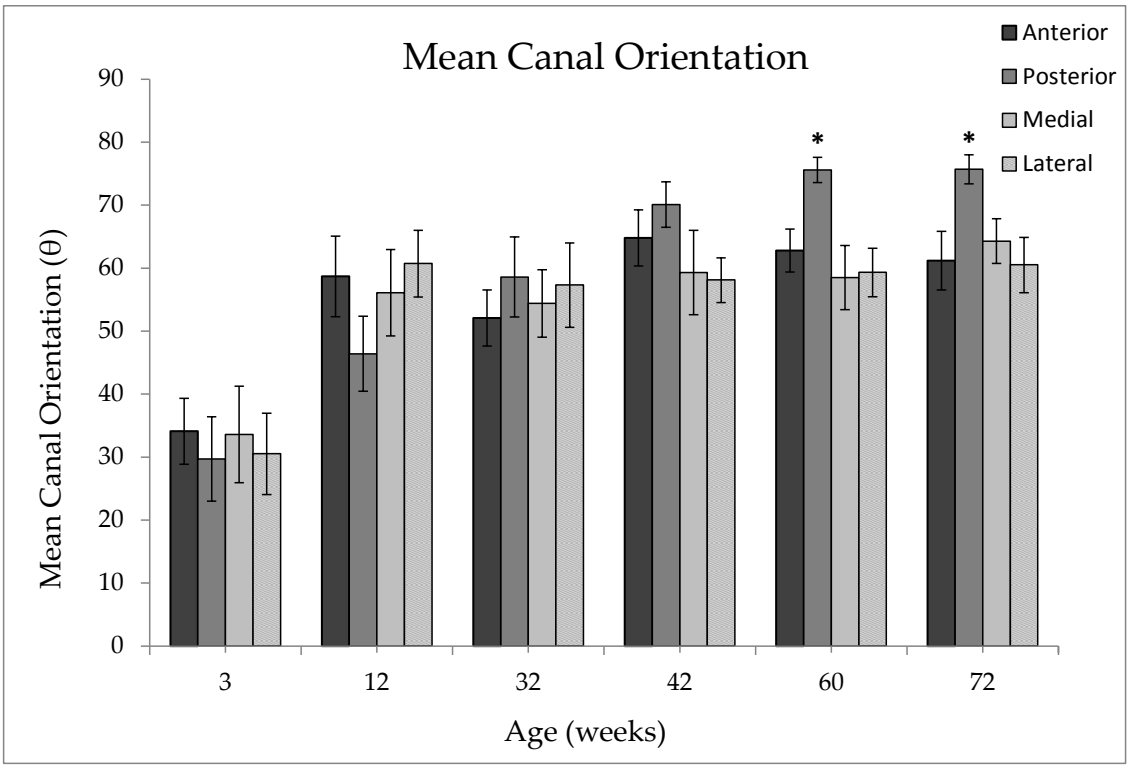

Figure 7. Age-related changes in mean canal orientation at various anatomical sites. *denotes values statistically significantly different ($p < 0.05$) from another site according to Tukey's HSD test.

1.4 DISCUSSION

At the macrostructural level, the tibial mid-diaphysis of the Sprague-Dawley rat displayed a rapid increase in size and volume from 3 weeks of age to 12 weeks of age. This increase can be attributed to a period of rapid growth in rats observed between 4 and 8 weeks of age, as observed by Roach *et al.* in Wistar rats (Roach *et al.*, 2003) and McHugh *et al.* (McHugh *et al.*, 2002) and Bennell *et al.* (Bennell *et al.*, 2002) in Sprague-Dawley rats. During this period, bone undergoes an increase in radial growth, corresponding to the increase in total tissue volume observed between 3 and 12 weeks of age. Following the period of rapid growth, the growth rate of the tibia gradually decreases until it virtually ceases after 28-30 weeks of age (Walker *et al.*, 1972). This same growth phenomenon describes the initial increase in cortical thickness and cortical bone volume observed between 3 and 12 weeks of age. Following the rapid growth period (samples 12 weeks and older), these parameters remained relatively constant and did not exhibit statistically significant changes with age ($p > 0.05$). The gradual decrease in cortical

thickness observed coincides with previous work done by Li *et al.* (Li *et al.*, 1991) who found that female Sprague-Dawley rats between the ages of 3 and 16 months (~13 and 70 weeks) display no changes in tibial cortical area with age but rather a redistribution of bone mass from the endosteal region to the sub-periosteal region of the tibia. This redistribution of bone mass results in a gradually thinning of the cortical wall as displayed in Table 1. The gradual decrease in cortical thickness from 12 to 72 weeks of age yields the decrease in cortical bone volume observed between that same age span. This redistribution of mass from the endosteal region to the sub-periosteal region also results in a net deposition of bone mass further from the neutral axis of the bone, a compensatory mechanism designed to preserve structural strength and stiffness as the tissue level properties of bone degrade with age (Buhl et al., 2002). This mass redistribution results in the gradual increase in polar area moment of inertia as seen in Table 1.

It is well documented that bone formation rate and the activity of the bone-forming cells within the basic multicellular unit (BMU) are correlated with bone perfusion and the development of the vascular network (Whiteside *et al.*, 1977; Kirkeby *et al.*, 1991; Barou *et al.*, 2002). Therefore, in order for bone to sufficiently vascularize during a period of rapid growth, it is necessary that the canal network grows and develops. This growth is evidenced by the initial increase in canal number density between 3 and 12 weeks of age as seen at the microstructural level (Table 2). During the period of rapid growth between 3 and 12 weeks, the vascular network grows and densifies to supply sufficient blood, nutrients, and oxygen to bone and the bone-forming cells in the BMU. Following the rapid growth period, there is a gradual decrease in the canal number density. A decrease in canal number density indicates suppression in the degree of canal network formation that is perhaps related to a reduced degree of bone vascularization and bone formation activity during the advancement into maturation and senescence (Gerber *et al.*, 1999; Matsumoto *et al.*, 2007). This phenomenon is illustrated in Figure 8, which displays the densification of the canal network from 3 to 12 week and the subsequent suppression at 60 weeks. This finding coincides with previous work done by Hagaman *et al.* (Hagaman *et al.*, 1991), who used scanning electron microscopy (SEM) to determine that the

number and density of vascular canals within Wistar rats decreases from 6 months (~26 weeks) to 24 months (~104 weeks) of age.

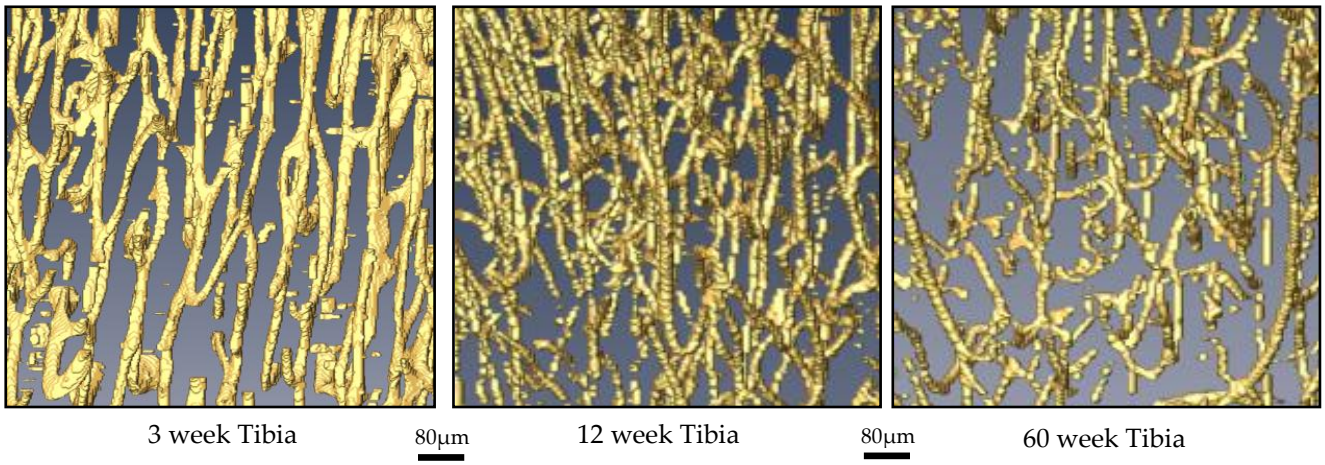

Figure 8. 3D reconstructed mid-diaphyseal canal network obtained by negative imaging. The data have been obtained at 1.0μm resolution. Age-related changes in canal network density and mean canal size can be observed between the age groups.

Although the density of the canal network increases, there exists an overall decrease in canal volume density with age. Therefore, the contribution of the canal network to the overall porosity of bone decreases with age. The decrease from 6.13% at 3 weeks to 2.72% at 12 weeks is statistically significant ($p < 0.05$) which the gradual decrease exhibited after 12 weeks of age is not ($p > 0.05$). The significant decrease in canal volume density from 3 to 12 weeks results from a morphometric change in canal geometry during this same age span. Namely, the mean canal diameter from 3 to 12 weeks significantly decreases from 29.7μm to 21.1 μm, causing a corresponding statistically significant decrease in mean canal volume (Figure 8). Therefore, although the density of canals within the network increases, the mean diameter (and therefore volume) of these canals decreases, resulting in an overall decrease in canal volume density.

As shown in Table 2, mean canal orientation increases with age, signifying that canal branches within the cannular network become more radially-oriented with age. This change in mean canal orientation is illustrated in Figure 9. Following a period of rapid growth up to about 8 weeks of age (McHugh *et al.*, 2002; Bennell *et al.*,2002), the growth plate in the tibia of the rat decreases in width, corresponding to decreased longitudinal growth (Greenspan *et al.*, 1949;

Schoenle *et al.*, 1982). After approximately 17 weeks of age, the tibia enters a longitudinal growth plateau (Becks *et al.*, 1945). Near 28-30 weeks of age, bone essentially ceases its longitudinal growth (Walker *et al.*, 1972); however, bone continues to remodel and redistribute its mass as it resorbs from the endosteal region and deposits on the sub-periosteal region. This change in dynamic from longitudinal growth to exclusively radial redistribution of mass could explain the change in spatial arrangement in the canal network. As less energy is required for longitudinal growth, canals become more radially oriented to continue and make more efficient the transport of blood and nutrients to both the endosteal and periosteal regions.

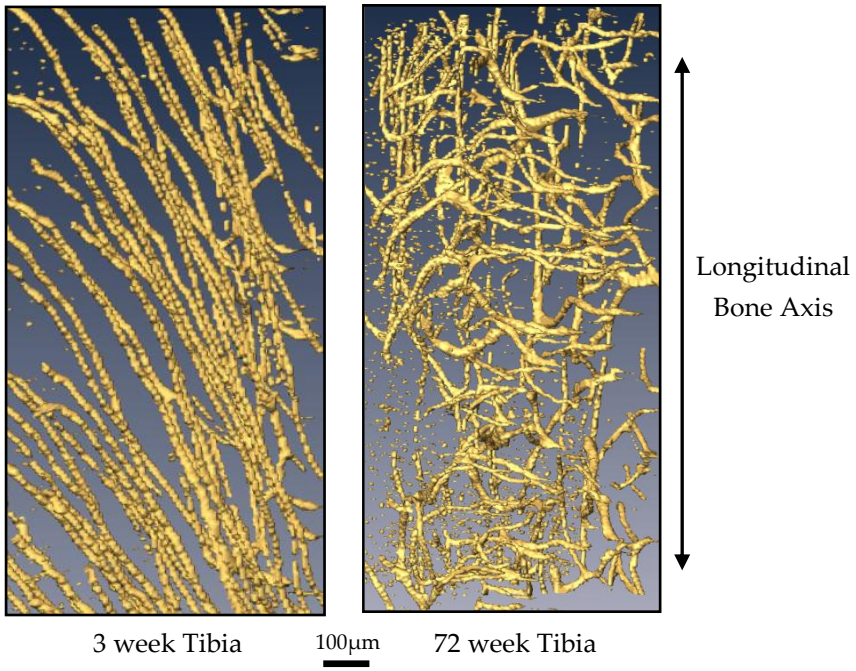

Figure 9. Canal network within the posterior region of cortical bone from 3 week and 72 week samples. The data have been obtained at 1.0μm resolution. Note the difference in canal network spatial arrangement. There exists preferential longitudinal alignment of canals within the 3 week sample. The canal network becomes more radially-oriented with age, as evidenced by the 72 week sample.

Regarding the dependence of microstructural parameters on anatomical site, the medial region of the tibia had a lower canal number density and cannular porosity (porosity due to canals only) than the other sites. This result becomes less apparent at older ages (60+ weeks) as the cannular porosity and number density of canals increases and becomes comparable to other regions. At these older ages, there is also a decrease in canal number density and cannular

porosity in the posterior region if the tibia. Similar work done by Schneider *et al.* on the determination of ultrastructural properties of murine cortical bone revealed a similar site-dependency of canal number density and canal volume density within femoral bone. Particularly, Schneider *et al.* found there to be a significant difference between the anterior and posterior regions, citing a 4-fold decrease in canal volume density and a 5-fold decrease in canal number density in the posterior region as compared to the anterior region (Schneider *et al.*, 2007). An analogous site-dependency was found by Matsomoto *et al.* in rat tibiae harvested from 3 and 4 week old rats (Matsumoto *et al.*, 2010). Using monochromatic synchrotron radiation CT (SRCT), Matsumoto and colleagues found the posterior region of the tibia to be less porous than the anterior region. The site dependence of cortical microstructure was also investigated in turkey ulnae, where it was discovered that the cortical region containing the lowest cannular porosity was also the region subjected predominantly to compression (Skedros *et al.*, 2003, 2004). Therefore, in order to accurately examine the causality of anatomic differences in the canal network, information on the habitual loading of the rat tibial diaphysis in vivo is required. This is beyond the scope of the present study.

Although there existed differences in canal number density and canal volume density between regions, the parameters describing the single basic elements of the canal network (mean canal volume, mean canal diameter, and mean canal length) were independent of anatomical location. These findings are consistent with a similar study done by Schneider *et al.* in which same conclusion was drawn regarding the site-independence of these element-based parameters within murine femora (Schneider *et al.*, 2007). Although Schneider and colleagues were comparing differences between two strains of mice, the cannular element-based parameters within each strain displayed no site-dependence. While parameters describing cannular geometry were independent of site, the spatial orientation of these canals was shown to be site-dependent. Specifically, in older samples (42 weeks+), the posterior region of the tibia contained canals that were more radially-oriented (greater mean canal orientation) than the other regions, and these differences were significant at 60 and 72 weeks of age. Schneider *et al.* also determined there to be a site-dependence of mean canal orientation within mouse femora,

although those findings found the anterior and medial regions to contain canals with a greater mean orientation.

Until recently, the vast majority of analysis of osteocyte lacunae has been restricted to the 2-dimensional realm and has been based on the microscopical analysis of histological bone sections. Although 3-dimensional analysis has been relatively restricted up until this point, osteocyte lacunae have been analyzed and characterized since the development of the methodology for dynamic bone histomorphometry (Schneider *et al.*, 2007). As seen in Table 3, lacuna number density was found to be independent of age. Previous studies investigating lacunar density have reported conflicting results. Within human bone, some have determined that lacunar density decreases with age (Baud *et al.*, 1973; Mullender *et al.*, 1996a; Qiu *et al.*, 1998) while others have found that it increases with age or remains constant (Vashishth *et al.*, 2000a). Studies of human vertebral trabecular bone and femoral cortical bone done by Vashishth *et al.* have demonstrated that the relationship between lacuna number density and age is dependent on gender and is tissue specific (Vashishth *et al.*, 2000a,b). This could partially account for the discrepancy between results obtained by Mullender and colleagues and those found in this study. Specifically, Mullender *et al.* estimated the osteocyte number density in rats to be approximately 93,000mm^{-3} (Mullender *et al.*, 1996b). Although this estimation differs significantly from the average lacuna number density calculated in this study (~42,000mm^{-3}), it is important to note that Mullender *et al.* analyzed femoral cancellous bone as compared to the tibial cortical bone analyzed in this study. Discrepancies in values can be attributed to differences in strain as well (Wistar vs. Sprague-Dawley).

The osteocyte lacunae were flattened and ellipsoidal in shape, similar to lacunae morphology determined previously (Aarden *et* al., 1994; McCreadie *et al.*, 2004; Schneider *et al.*, 2007). As shown in Table 3, the lacunae element-based parameters are independent of age. Similar results have been reported previously for human bone. Specifically, osteocyte lacuna size has been shown to vary little with age in human alveolar bone and femoral cortical bone (Baud *et al.*, 1973; Qiu *et al.*, 1998). The average lacunae volume of ~290μm^3 found in this study is comparable to values reported by others for mice. Wang *et al.* reported a mean lacuna volume

of ~200-700 μm^3 within the tibiae of mice, and Schneider *et al.* reported mean lacuna volumes of ~200-300 μm^3. It is important to note that, with the exception of the work of Schneider *et al.*, most of the mean osteocyte lacuna volume values reported in literature are calculations based on 2-dimensional histological lacuna area measurements (Sissions *et al*., 1990). In addition to size, the spatial orientation of lacuna also proved to be independent of age. In general, osteocyte lacunae orientation has been found to be dependent on collagen fiber organization (woven or lamellar bone) and, in several cases, type of bone (long or flat). To state explicitly, osteocyte lacunae within woven bone have more of a spherical shape while those within lamellar bone are more ellipsoidal in shape (Remaggi *et al.*, 1998), as found in this study. Lacunae within the mouse have been reported to vary between long and flat bones, exhibiting an elongated morphology and major axis aligned parallel to the long axis of the bone (Vatsa *et al.*, 2008; Schneider *et al.*, 2007). These findings coincide with those in this work. Namely, lacunae were mainly longitudinally oriented with their major axis parallel to the long axis of the tibia.

The results of this study reveal a positive relationship between canal number density and bone size. Specifically, canal number density scales positively with cortical thickness and cortical bone volume. However, lacunar morphometry does not scale with bone size. Specifically, mean canal volume, mean canal volume density, and mean lacuna length do not scale with bone size.

Study Limitations

It is important to note that rats, unlike humans, rarely undergo osteonal remodeling. Therefore, within rat bone, regions of low-mineralized concentric lamellae surrounding a canal are virtually non-existent. Additionally, bone within rats reaches full mineralization more rapidly as compared to humans (Jowsey *et al.*, 1964), so it is not necessarily the case that regions surrounding canals exhibit low mineralization. For these reasons, the author cautions against a direct comparison between the rat canal network and the network found within human bone, as this comparison may be misleading. Furthermore, the analysis of this study was limited to the assessment of cortical bone within the rat tibia only. Further work needs to be completed to

determine differences between various bone types and species as well as the applicability of this rat model to human bone.

1.5 CONCLUSIONS

This study provided an assessment of cortical bone within the rat at different hierarchical levels. The results of this study give new insights into the cortical network morphology within the rat and how this network changes with age. To the knowledge of the author, this study is the first to analyze and quantify the cortical canal network morphology within the rat and assess changes within this network as a function of age. Through the use of a high resolution desktop micro-CT system and quantification software, intracortical porosity within the rat has been decomposed into the canal network and the osteocyte lacunar system, and each of these have been quantified using new cortical morphometric indices to describe their size, shape, and spatial orientation. The results of this study serve as valuable inputs into the computational modeling of bone at different hierarchical scales and will help provide new insights into the assessment of bone quality in the future.

CHAPTER 2: THREE-POINT BENDING AND MICROINDENTATION TESTING OF RAT CORTICAL BONE

2.1 INTRODUCTION

Bone is a dynamic, living tissue whose composition and structure are influenced by its function. The functional demands made upon bone influence its physical characteristics, ultimately affecting its mechanical properties (Buckwalter *et al.*, 1995; Meyers *et al.*, 2008; Fratzl *et al.*, 1992, 2007). Characterization of these properties is important as it aids in the understanding of bone pathologies and their corresponding treatments. For this reason, the mechanical properties of human and animal bone alike have been extensively studied in the past (Vanleene *et al.*, 2007). Many factors affecting the mechanical properties of bone have been identified including porosity (Currey *et al.*, 1988; Martin *et al.*, 1989; McCalden *et al.*, 1993), mineral content (Currey *et al.*, 1984, 1996), and the organization of collagen fibers (Lee *et al.*, 1977; Zioupos *et al.*, 2001; Morris *et al.*, 2004).

The rat has gained acceptance as a model of bone biology studies and is often used to investigate changes in bone structure and physio-chemical composition due to disease (Peng *et al.*, 1997; Han *et al.*, 1998; Jamsa *et al.*, 2002) and physical activities (Mosley *et al.*, 1997; Umemura *et al.*, 1997; Kannus *et al.*, 1996). Aging is a natural process that also alters bone properties and is therefore the interest of many studies. In this study, the rat model was chosen for the investigation of bone mechanical properties due to the availability of a wide range of sample age groups.

The quantification of mechanical properties has been achieved through the use of various experimental testing techniques including compression testing (McCalden *et al.*, 1993; Yeni *et al.*, 2004), tensile testing (Kotha *et al.*, 2007; Ramazan, 2007), and bending testing (Bagi *et al.*, 2006; Leppanen *et al.*, 2006; Margolis *et al.*, 2006). These techniques, although useful, typically only provide for the determination of properties at the organ, or whole bone, level. More recently, the investigation of local properties within bone is becoming more common with the usage of microindentation (Johnson *et al.*, 2007; Zwierzak *et al.*, 2009; Gardner-Morse *et al.*, 2010)

and nanoindentation (Swadener *et al.*, 2001; Fan *et al.*, 2002; Mittra *et al.*, 2006) techniques. As opposed to the tensile and compression testing techniques mentioned previously, indentation testing can be conducted on samples of unspecified geometry, eliminating the need for extensive sample preparation. Additionally, indentation testing is localized, so only a small region of a sample is damaged with each indentation, allowing for multiple indentations per sample without completely destroying it.

An innovative and novel microindentation technique recently developed, termed reference point indentation (RPI), has been utilized to gain insight into material properties using a unique indentation procedure (Hansma *et al.*, 2006, 2008; Randall *et al.*, 2009; Diez-Perez *et al.*, 2010). RPI is a minimally invasive technique that allows for the *in vivo* assessment of bone tissue strength (Diez-Perez *et al.*, 2010). Among other measurements, the technique is capable of measuring a unique parameter, the indentation distance increase (IDI), that is correlated with crack growth toughness and provides insight into a bone's resistance to fracture (Hansma *et al.*, 2008; Diez-Perez *et al.*, 2010). The RPI technique is utilized in this study to provide information about several mechanical properties of rat bone. Properties found using the RPI technique will be compared to those found using a traditional mechanical testing technique, the three-point bending technique. Variations in these mechanical properties with age will be studied, and the BioDent™ (BioDent™ H, Active Life Scientific, Santa Barbara, CA) instrument will be used to employ the RPI technique.

Previous studies have used a wide range of measurement techniques, rat strains, and ages, making it difficult to fully understand the impact of age on the mechanical properties of bone. Moreover, most studies focus on the fracture properties of older rat bone. This study will investigate changes in the properties of Sprague-Dawley rat bone from growth and into senescence, possibly elucidating trends in bone growth and development at older ages. Furthermore, by comparing properties gleaned from traditional three-point bending tests to those obtained using the RPI technique, usage of the RPI technique can be validated.

2.2 MATERIALS AND METHODS

2.2.1 SAMPLE PREPARATION

Tibiae were excised from female Sprague-Dawley rats obtained from control rats of previous studies. The rats ranged from infant to adult and included ages of 3 weeks (*n*=10), 12 weeks (*n*=8), 32 weeks (*n*=8), 42 weeks (*n*=6), 60 weeks (*n*=4), and 72 weeks (*n*=4). The background of each previous study was considered to ensure that its proceedings had no effect on the factors investigated in the current study. After harvesting and soft tissue removal, the bones were wrapped in gauze and soaked in a 0.1M phosphate buffered saline (PBS) solution to prevent dehydration. The samples were then stored at -20°C in sealed freezer bags. The effect of this storage protocol on bone has been studied previously and shown to have no effect on the mechanical properties of bone (Pelker *et al.*, 1984; Sedlin *et al.*, 1966).

2.2.2 THREE-POINT BENDING TESTING

24 hours prior to mechanical testing, bone samples were thawed to room temperature and kept wrapped in saline-soaked gauze at all times except during handling and testing procedures. Three-point bending tests were conducted as per the ASABE Standard for Shear and Three-Point Bending Test of Animal Bone (ANSI/ASAE S459). Tests were performed using an MTS Insight Elecromechanical Uniaxial Testing Machine (MTS Systems, Eden Prairie, MN, USA). Whole bone tibiae were placed on the lower fulcra (stainless steel plates with radii of 4mm) with a support span length of 20mm (10mm for 3wk samples) to maintain a support span to test specimen diameter ratio of greater than 10 in order to minimize deformation due to shear stresses. Prior to actual testing, a small stabilizing preload (0.5N) was applied to the anterior surface of the tibia at a rate of 0.1mm/min using a loading bar (stainless steel plate with a radius of 2mm). The plate was oriented perpendicular to the longitudinal axis of the bone and positioned at the midpoint between the lower fulcra. The load was applied at the mid-diaphysis in an anterior-posterior (AP) direction at a crosshead loading speed of 10mm/min. Documentation of crosshead speed is important as bone is a viscoelastic material and strength is strain-rate dependent (Carter *et al.,* 1977; Robertson *et al.,* 1978; Currey *et al.,* 1988; Courtney *et*

al., 1993; McElhaney *et al.*, 1966). The bones were tested until failure occurred. Data were recorded and processed using TestWorks 4 (MTS software) and were used to construct a load-displacement curve. The bending stiffness (N/mm) was determined from the load-deformation curve (Figure 10), as described previously (Lind *et al.*, 2001; Lundberg *et al.*, 2007). Ultimate bending strength (MPa) and apparent modulus (GPa) were calculated as described in ANSI/ASAE S459. Briefly, these biomechanical indices are defined as follows: bending stiffness is the maximum slope of the linear portion of the load-deformation curve; ultimate bending strength is the maximum stress experienced by the bone; and apparent modulus is the modulus of elasticity (shear deflection was assumed negligibly small compared to bending deflection). As described previously (ANSI/ASAE S459), area moment of inertia calculations were done by measuring bone dimensions at the mid-diaphysis and modeling the tibial cross-section as a hollow ellipse.

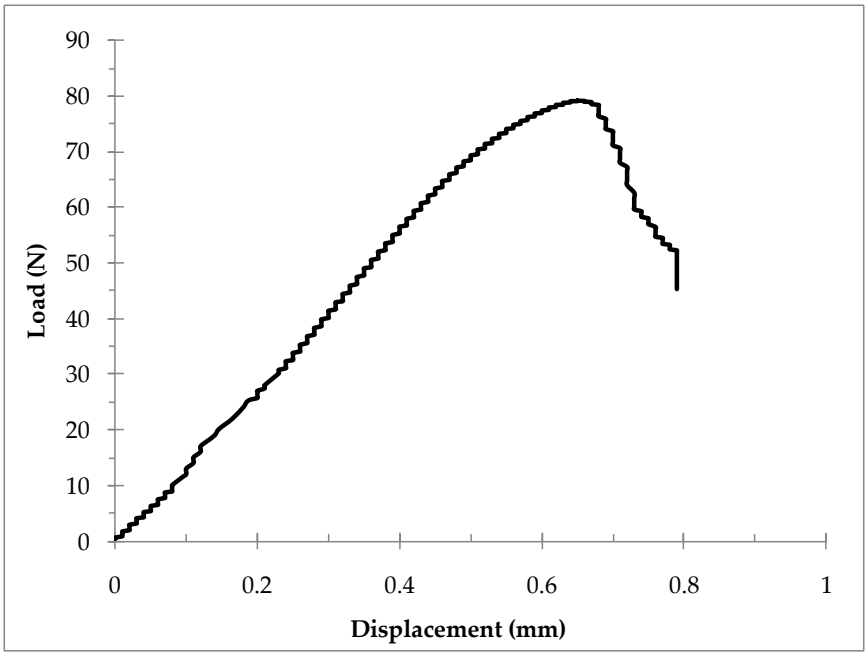

Figure 10. Typical three-point bending test force-deformation curve

2.2.3 MICROINDENTATION INSTRUMENT

The BioDent™ indentation instrument is capable of *in vivo* indentation testing of bone specimens and was developed to directly measure bone tissue properties by employing a microindentation technique (Randall *et al.*, 2009; Hansma *et al.*, 2006, 2008, 2009). Specifically, it

is capable of measuring bone tissue strength as well as fracture resistance (Diez-Perez *et al.*, 2010).

The technology consists of an assembly of two concentric needles. An outer hypodermic needle acts as a reference probe, resting on the outer surface of a sample and establishing a reference point at the site of indentation. This reference point allows for measurements of displacement. The inner needle slides relative to the reference probe and acts as an indentation test probe that indents into bone for the determination of mechanical properties. The inner test probe repeatedly indents the bone sample, advancing deeper into the bone with each subsequent indent. Previous work by others employs an indentation scheme of 10 to 20 cycles, with a total cycle time of 500ms for each indent (Hansma *et al.*, 2008; Diez-Perez *et al.*, 2010). Force is applied via the test probe using a modified triangular waveform, as described previously (Diez-Perez *et al.*, 2010). Briefly, there is a linear increase in force for the first one-third of a cycle. Then, maximum force is held for one-third of a cycle to allow for creep measurement. Finally, the indentation cycle is completed with a linear decrease in force for the remaining one-third of a cycle.

2.2.4 MICROINDENTATION TESTING

Since the BioDent™ instrument is capable of *in vivo* testing, little sample preparation is necessary following excision and soft tissue removal. 24 hours prior to testing, bone samples were thawed to room temperature and kept wrapped in saline-soaked gauze to maintain bone hydration. Due to limited time and instrument access, only one tibia sample was tested from each of the following age groups: 3 weeks, 12 weeks, 32 weeks, 60 weeks, and 72 weeks. During testing, samples were submerged in PBS and stabilized using an adjustable clamp. Indentations were made on the exterior surface of the bone, and force was applied in a direction perpendicular to the long axis of the bone. Indentations were made at 5 locations on the lateral side of each tibia, beginning at the tibio-fibular junction and proceeding in the proximal direction. At each location, 20 indents were made. Indents were load-controlled to a maximum force of 11 N, as recommended previously (Hansma *et al.*, 2008; Diez-Perez *et al.*, 2010).

The indentation cycles yield load-displacement curves, the first and last of which are displayed after testing, as shown in Figure 11 (Rasoulian, 2010). Three indentation parameters were measured using the curves. Indentation distance increase (IDI) is a measure of the increase in indentation distance in the last cycle compared to the indentation distance in the first cycle (Figure 11). In addition to IDI, stiffness was determined by averaging the slopes of each unloading curve for all cycles. Finally, mean energy dissipation (a measure of hysteresis) was determined by calculating the area between the loading and unloading curves for each cycle and averaging across all cycles (excluding the first and second cycles).

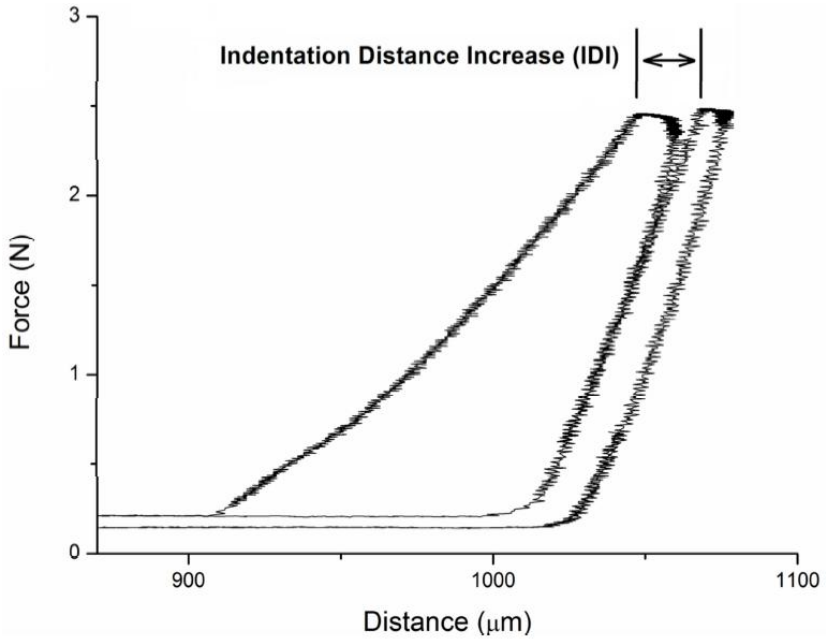

Figure 11. Force-Distance curve representing the output obtained from the BioDent™ RPI instrument. Indentation distance increase (IDI) is a measure of the increase in indentation distance in the last cycle compared to the indentation distance in the first cycle.

2.2.5 STATISTICAL ANALYSIS

To test for differences in mean parameter values between age groups, OriginPro 8.1 (OriginLab Corp. Northampton, MA) statistical analysis was used to conduct one-way analysis of variance (ANOVA). Following one-way ANOVA testing, Tukey's honestly significant difference (HSD) tests were performed as a post hoc analysis for pairwise comparisons among means to explicitly determine which parameters were significantly different from one another.

2.3 RESULTS

2.3.1 THREE-POINT BENDING TESTING

As age increases, the ultimate bending stress required to fracture bone decreases, as illustrated in Figure 12. There is a slight, albeit statistically insignificant decrease in ultimate bending stress from 270 MPa at 3 weeks to 243 MPa at 12 weeks of age. Ultimate strength values for age groups 12 weeks, 32 weeks, and 42 weeks were relatively constant. Between the 42 week and 60 week samples, there was a 32% decrease in ultimate bending strength, a statistically significant drop ($p < 0.05$). There also existed a statistically significant difference in ultimate bending strength between the 72 week sample group and all other groups, excepting the 60 week samples.

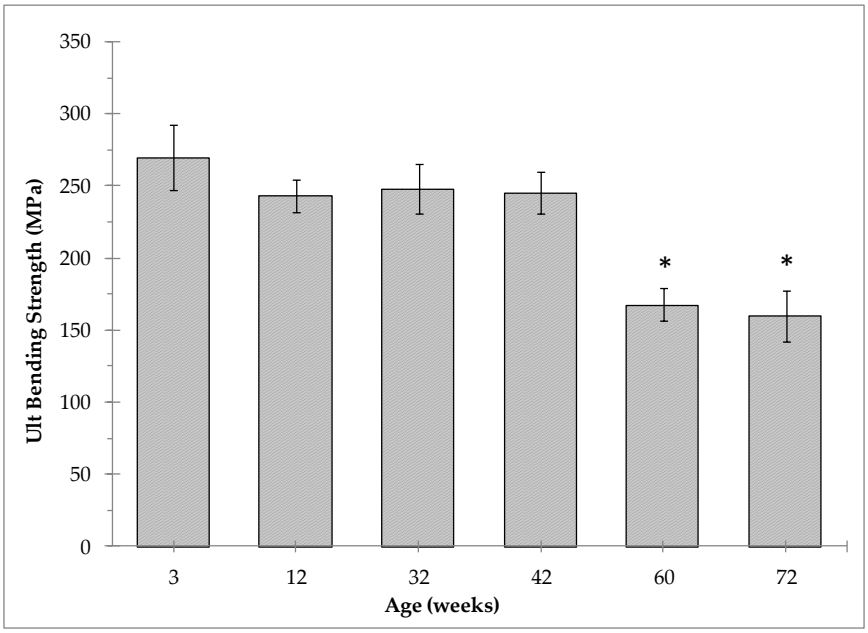

Figure 12. Comparison of rat tibiae ultimate bending strength between various age groups. There exists a statistically significant drop in ultimate bending strength between the 42 week and 60 week age groups, while no significant differences existed between the 3 week, 12 week, 32 week, and 42 week samples ($p > 0.05$).

Figure 13 illustrates the variation of bending stiffness between the various age groups. Overall, there is an increase in bending stiffness with age. There is a sharp increase in stiffness between both the 3 week and 12 week samples as well as between the 12 week and 32 week

samples. These increases of 314% and 70% are statistically significant ($p < 0.05$). After 32 weeks of age, there is a more gradual increase in bending stiffness, and differences between mean bending stiffness values are not statistically significant ($p > 0.05$). As discussed below, area moment of inertia is an important factor affecting the bending stiffness of bone. To more completely understand changes in bending stiffness as a function of age, changes in the area moment of inertia of each bone was investigated. Figure 14 illustrates the dependence of bone age on its area moment of inertia.

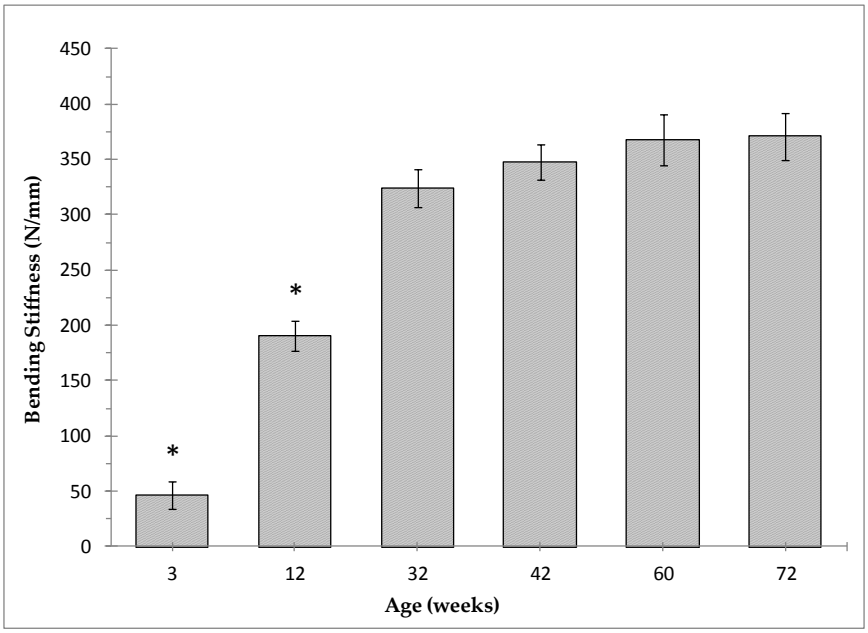

Figure 13. Variation of rat tibia bending stiffness as a function of age. Bending stiffness increased with age. Statistically significant differences in mean bending stiffness were observed in the 3 week and 12 week age groups when compared to the 32 week, 42 week, 60 week, and 72 week groups ($p < 0.05$).

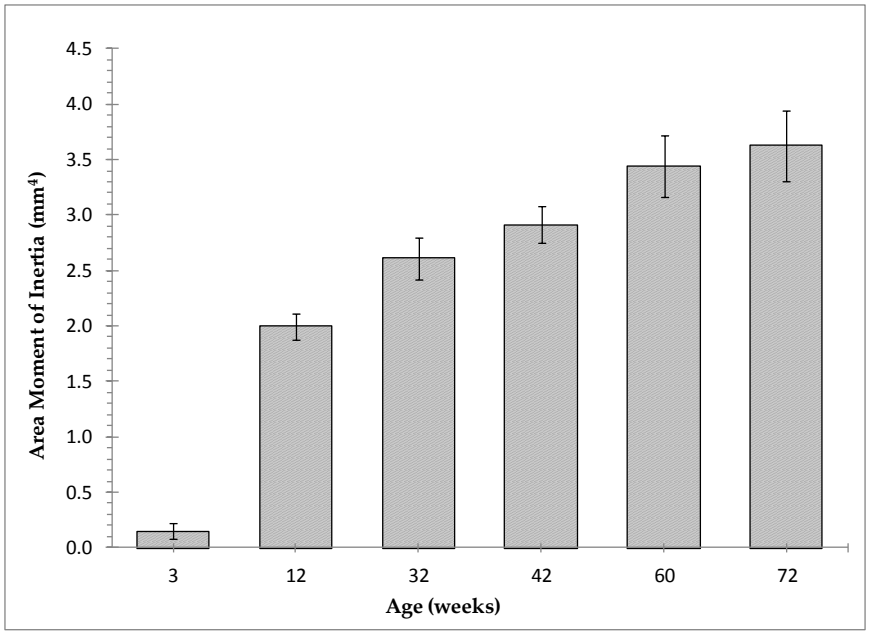

Figure 14. Variation of area moment of inertia in rat tibia during growth and senescence. Area moment of inertia increases rapidly initially and more gradually from 12 weeks to 72 weeks of age. Statistically significant differences in area moment of inertia existed between all age groups excepting between 32 and 42 weeks as well as between 60 and 72 weeks ($p < 0.05$).

As illustrated by Figure 15, the tibial apparent modulus of elasticity increases with increasing age. The increase is very pronounced initially as there is a four-fold increase in modulus values between 3 weeks and 12 weeks of age. Following this rapid increase is a continued gradual increase from 3.99 GPa at 12 weeks to 4.27 GPa at 42 weeks. After 42 weeks of age, apparent modulus values level off at approximately 5.5 GPa. Only the 3 week age group exhibited a statistically significant difference in mean apparent modulus as compared to the other age groups ($p < 0.05$).

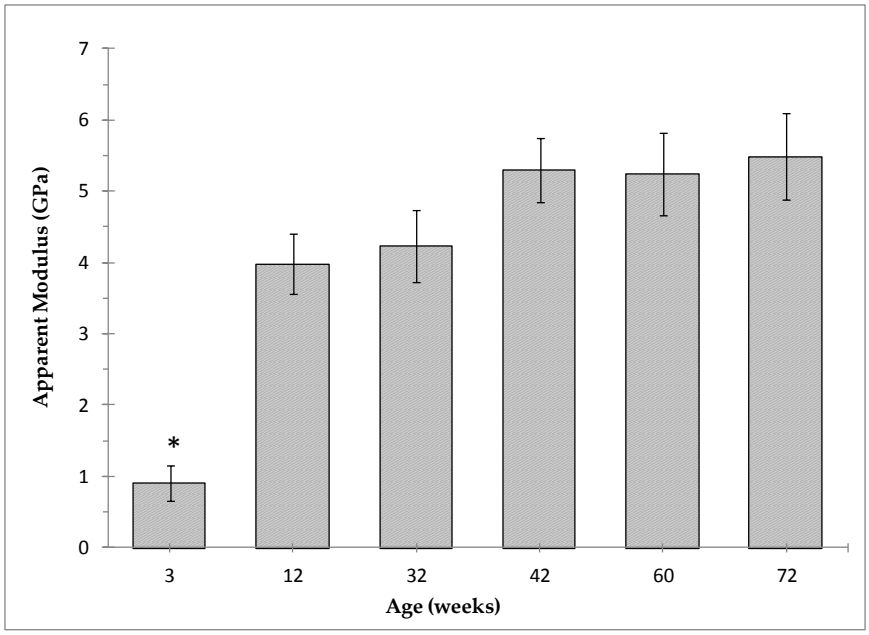

Figure 15. Change in apparent modulus of rat tibia as a function of age. There is a statistically significant increase in apparent modulus from 3 to 12 weeks ($p < 0.05$), followed by a gradual increase and eventual leveling off into senescence.

2.3.2 MICROINDENTATION TESTING

The trend of decreasing IDI with age is apparent, as illustrated in Figure 16. IDI decreases with each consecutive age group, and the largest drop in IDI was a 24% decrease from 17.4μm at 12 weeks to 13.2μm at 32 weeks of age. This drop was statistically significant ($p < 0.05$). Following the rapid decrease in IDI among the three youngest age groups, the decrease in IDI becomes more gradual before finally dropping to 10.6μm for the 72 week age group. A similar trend is observed for MED (Figure 18), which also decreases with age. Again, the largest drop is observed between the 12 week and 32 week samples. This decrease from 96.4 μJ at 12 weeks to 64.2 μJ at 32 weeks represents a statistically significant drop of 33.4% ($p < 0.05$). Conversely, as shown by Figure 17, stiffness values do not share this trend. Stiffness initially increases from 556 N/mm for the 3 week age group to 745N/mm for the 12 week age group, a statistically significant increase of approximately 34%. Following this marked increase, there is no apparent trend as stiffness values remain relatively constant.

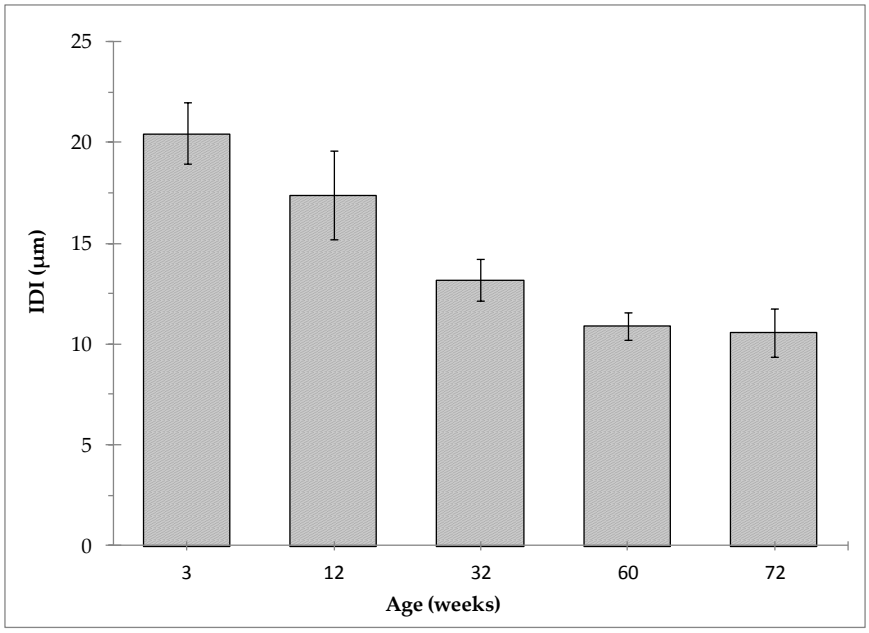

Figure 16. Change in indentation distance increase (IDI) as a function of age. IDI steadily decreases with age, the largest drops occurring between the first three age groups. The 24% decrease observed between the 12 week and 32 week age groups is statistically significant ($p < 0.05$).

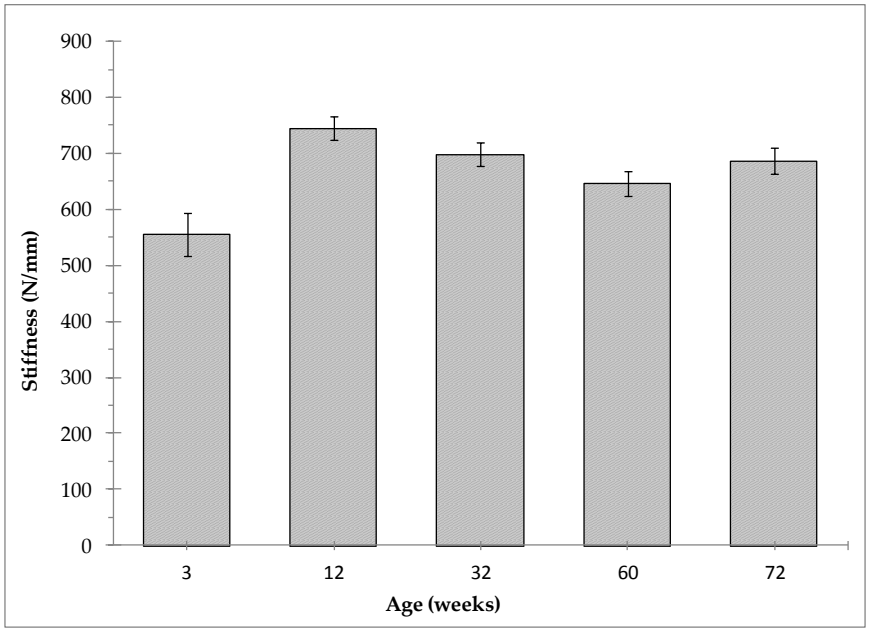

Figure 17. Change in rat tibia stiffness, as measured by microindentation testing, as a function of age. Following a sharp statistically significant increase in stiffness initially, stiffness values gradually decrease before a final increase within the 72 week age group.

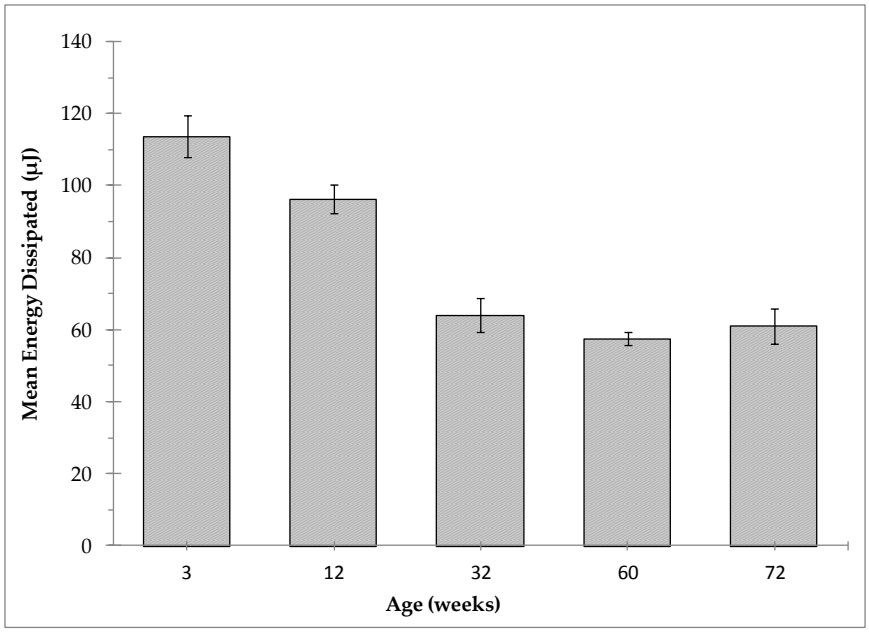

Figure 18. Change in mean energy dissipation (MED) with increasing age. Between the 3, 12, 32, and 60 week samples, there exists a marked decrease in MED with age. Decreases in MED are statistically significant among each of the 3, 12, and 32 week age groups ($p < 0.05$).

2.4 DISCUSSION

There are two important factors to consider when investigating the structural properties of bone: geometry and tissue material properties. As illustrated by Figure 14, there were significant geometrical changes in the tibiae with age. Namely, area moment of inertia (MOI) values increased with advancing age. This finding is a result of a redistribution of mass around the medullary cavity as bone ages. Due to a periosteal bone accretion and simultaneous endosteal bone loss, there is a net deposition of bone mass further away from the bone's neutral axis, enhancing its structural properties. This effect has been well-documented in previous studies (Buhl *et al., 2002*; Hagaman *et al.,* 1991; Kiebzak *et al., 1988*). Since stiffness is an extensive material property, directly proportional to a material's shape and size, the observed increase in MOI with age accounts for the increasing stiffness seen in Figure 13.

Although it has been shown previously that MOI is positively correlated with the structural properties and performance of bone in bending (Mow *et al.*, 1994), results from the present study reveal that the older tibiae were not stronger than the younger tibiae, even

though the older tibiae exhibited greater MOI values. This is due to the fact that, as mentioned previously, material properties also contribute to the structural integrity of bone. A decline in the material properties of the constituent bone tissue with age could account for the decreased stress-bearing capacity of the older tibiae. This observed decreasing ultimate stress with age (Figure 12) correlates well with what has been demonstrated previously in rats (Bak *et al.,* 1989; Buhl *et al.*, 2002; Kiebzak *et al.,* 1988). Due to the age-related decline in material properties, the aforementioned increase in bone size may be a compensatory mechanism set forth to offset this decline in material properties and maintain structural rigidity.

During analysis of bending test results, although material properties were calculated after normalizing for bone geometry, these material properties were still measured indirectly. Therefore, it is important to compare the present findings with those of similar investigations employing direct measurement techniques. The results presented in this study are similar to previous investigations that also found a gradual decline in bone material properties with age (Burstein *et al.*, 1976; McCalden *et al.*, 1993; Buhl *et al.,* 2002; Raab *et al.* 1990).

Bone tissue is composed of multiple phases: an organic collagen phase and an inorganic mineral phase, comprised of hydroxyapatite (Walsh *et al.*, 1994; Beuvelot *et al.*, 2010). As bone ages from infancy into adulthood, the volume fraction and modulus of the hydroxyapatite mineral constituent increase (Bonfield *et al.*, 1973). This age-related change explains the increasing modulus values observed in this investigation (Figure 15). However, as bone growth continues into senescence, elastic modulus begins to decrease due to an increase in porosity (McCalden *et al.*, 1993). This effect has been observed previously in rat bone (Kiebzak *et al.,* 1988; Buhl *et al.*, 2002). However, a decrease in modulus was not observed at older ages in the present study. This is due to the fact that the oldest age group of rats in this study had not yet experienced this increase in porosity. Indeed, the largest decreases in modulus with were observed in rats that were 24 months of age and older in the previously mentioned studies. The average life span of a rat is 2.5-3 years of age (Pass *et al.*, 1993), and female rats enter menopause at approximately 15 months (65 weeks) of age (Durbin *et al.*, 1966). Therefore, in this study, the

72 week age group had only begun menopause and perhaps had not yet experienced significant changes in bone structure that come with aging.

In addition to three-point bending tests, microindentation testing was also employed via the BioDent™ instrument to further characterize the mechanical properties (specifically fracture properties) of rat bone. The indentation procedure involves making repetitive indentations on the surface of bone using a micro-scale indenter. This indenter slides within a hypodermic needle that rests on the surface of bone and acts as a reference probe (Hansma *et al.*, 2009); therefore, the technique is referred to as reference point indentation (RPI). Techniques used previously to measure the fracture properties of bone are limited in that only the macroscale toughness of bone is reported. These techniques include single-edge notched beam testing (Lucksanasombool *et al.*, 2001; Yan *et al.*, 2007, 2008) and compact tension testing (Norman *et al.*, 1996; Feng *et al.*, 2000; Bingbing *et al.*, 2010). Additionally, classical indentation toughness measurement methods, including Vickers indentation fracture (VIF) test and the cube corner indentation fracture (CCIF) test, have been used for measuring the toughness of hard biological tissues such as bone and dentin (Marshall *et al.*, 2001; Mullins *et al.*, 2007). However, as outlined by Kruzic *et al.*, the use of these indentation methods is not suitable for quantifying the fracture toughness of materials because these methods utilize linear elastic fracture mechanics, the requirements of which may not be met when testing hard tissues such as bone (Kruzic *et al.*, 2009). Therefore, Kruzic *et al.* advised against employing these methods to investigate the fracture toughness of bone. Furthermore, experimentation with these previous techniques is done *in vitro*, requiring bone samples to be excised from a host body and tested remotely. Conversely, the RPI technique employed in this study is capable of *in vivo* measurements of bone material properties, potentially contributing to the assessment of bone fragility (Hansma *et al.*, 2008).

As outlined by previous studies (Diez-Perez *et al.*, 2010; Hansma *et al.*, 2008), although underlying mechanisms are not fully understood, it is generally accepted that IDI is a measure of damage resulting from repeated indentations. Diez-Perez *et al.* compared IDI measurements with crack growth toughness values for five samples of human cadaveric bone ranging in ages

from 17 to 74 years and found a strong negative Pearson correlation coefficient, revealing the existence of an inverse relationship between IDI and crack growth toughness. Specifically, higher IDI values and lower crack growth toughness are associated with bones that are more prone to fracture (Diez-Perez *et al.*, 2010). Hansma *et al.* investigated several model systems and found that samples with degraded mechanical properties yielded greater IDI values. Specifically, it was suggested that bone that is more easily fractured has larger IDI values (Hansma *et al.*, 2008).

As illustrated in Figure 16, IDI decreases with age, suggesting that as bone grows from infancy and into adulthood, it becomes less prone to fracture. This is expected since during growth and maturation, bone formation yields enhanced fracture properties. To fully understand this relationship, it is important to note the fracture toughening mechanisms that exist within bone. Crack propagation is governed by two classes of mechanisms: intrinsic and extrinsic. Intrinsic mechanisms are microstructural mechanisms that operate ahead of the crack tip to increase resistance to crack initiation. Conversely, extrinsic mechanisms act in the wake of the crack and function to shield the crack from the applied driving force and arrest crack propagation (Ritchie *et al.*, 2006; Launey *et al.*, 2010). In cortical bone, it has been suggested that osteons function to contribute to extrinsic toughening, thwarting crack growth by acting as barriers that redirect crack propagation (Nalla *et al.*, 2006). Furthermore, cement lines surrounding osteons often cause microcracks to arrest (O'Brien *et al.*, 2003, 2005) and are perhaps also responsible for crack bridge formation (Ritchie *et al.*, 2006). However, unlike humans, rats rarely undergo osteonal remodeling; therefore, osteons are virtually non-existent within rat bone (Jowsey *et al.*, 1964; Schneider *et al.*, 2007). IDI is inversely correlated with fracture toughness, so the decrease in IDI with age corresponds to an increase in fracture toughness (Figure 16). Since rat bone is typically devoid of osteons, perhaps another mechanism is contributing to this increased fracture toughness with age. In general, the lamellar bone that composes rat bone fulfills a variety of different mechanical functions, the specifics of which are not fully understood. However, it has been proposed that it acts as the "concrete" of the vertebrate skeleton (Weiner *et al.*, 1999). Each lamellar unit is composed of multiple layers, each

layer consisting of an array of aligned collagen fibers. As age increases, these collagen fibers continue to mineralize, which may account for the observed increase in fracture toughness. Although elder age groups were not available for analysis at the time of the study, it is expected for older rats entering menopause (72 weeks +) that fracture toughness begins to decrease with age due to increasing porosity and the deterioration of the collagen network strength and energy-absorption capacity (Burnstein *et al.*, 1976; Wang *et al.*, 1998, 2004).

The present study has limitations. The analysis of this study was limited to the assessment of bone within one animal, the rat. Furthermore, among the many bones existing within the rat, only the mechanical properties of the tibia in particular were investigated. Further work needs to be completed to determine differences between bone types and species as well as the applicability of the rat model to human bone. Finally, although the life span of the average rat is 2.5-3 years of age (Pass *et al.*, 1993), the oldest age group available at the time of this study was 72 weeks, the time at which female rats enter menopause and expectedly begin to experience a degradation in bone quality. A complete assessment of older age groups with the BioDent™ instrument is necessary to fully understand the effects of advanced aging on the properties of rat bone.

2.5 CONCLUSIONS

Changes in the mechanical properties of rat bone as a function of age were investigated. By conducting traditional three-point bending tests as well as a novel microindentation technique capable of *in vivo* testing, information including changes in apparent modulus, stiffness, mean energy dissipation, and ultimate bending strength as a function of age were reported. Additionally, a parameter unique to the BioDent™ testing instrument, the IDI, was used to infer the fracture toughness of bone at various ages. Although the pronounced trend observed in IDI measurements with age is promising, only one sample from each age group was able to be tested due to limited access to the BioDent™ instrument. A more thorough study is warranted to provide a better understanding of bone properties achieved using the BioDent™

and a more direct comparison of these results to those obtained using traditional mechanical testing techniques.

REFERENCES

Aarden, E.M., Burger, E.H., Nijweide, P.J., *Function of osteocytes in bone*. J Cell Biochem, 1994. **55**: p. 287-299.

Alkemper, J., Voorhees, P.W., *Quantitative serial sectioning analysis*. Journal of Microscopy, 2000. **201**: p. 388-394.

Bagi, C.M., Hanson, N., Andresen, C., *et al., The use of micro-CT to evaluate cortical bone geometry and strength in nude rats: Correlation with mechanical testing, pQCT and DXA*. Bone, 2006. **38**: pp. 136-144.

Bak, B., Andreassen, T.T., *The effect of aging on fracture healing in the rat*. Calcif Tissue Int, 1989. **45**: p. 292-297.

Barou, O., Mekraldi, S., Vico, L., Boivin, G., Alexandre, C., Lafage-Proust, M.H., *Relationships between trabecular bone remodeling and bone vascularization: a quantitative study.* Bone, 2002. **30**: p. 604–12.

Basillais, A., Bensamoun, S., Chappard, C., Brunet-Imbault, B., Lemineur, G., Ilharreborde, B., Ho Ba Tho, M.C., Benhamou, C.L., *Three-dimensional characterization of cortical bone microstructure by computed tomography : validation with ultrasonic and microscopic measurements*. J Orthop Sci, 2007. **12**: p. 141-148

Baud, C. A., *Histophysiology of the Osteocyte: An Introduction to the Morphometry of Peri-Osteocytic Lacunae.* Proc. 1st Workshop on Bone Morphometry,1973. p. 267–272.

Beuvelot, J., Bergeret, C., *et al., In vitro calcification of chemically functionalized carbon nanotubes*. Acta Biomaterialia, 2010. **6**: p. 4110-4117.

Becks, H., Simpson, M. E., Evans, H. M., *Ossification at the proximal tibial epiphysis in the rat. I. Changes in females with increasing age*. Anat. Rec., 1945. **92**: p. 109.

Bennell, K.L., Khan, K.M., Warmington, Forwood, M.R., Coleman, B.D., Bennett, M.B., Wark, J.D., *Age does not influence the bone response to treadmill exercise in female rats*. Med. Sci. Sports Exerc., 2002. **34**: p. 1958–1965.

Bingbing, A., et al., *An experimental approach on fracture behavior of cortical bones*. Chinese Journal of Theoretical and Applied Mechanics, 2010. **42**: pp. 1164-1171.

Bonfield, W., Clark, E.A., *Elastic deformation of compact bone*. Journal of Materials Science, 1973. **8**: p. 1590-1594.

Bonse, U., Busch, F., *X-ray computed microtomography (microCT) using synchrotron radiation (SR)*. Prog Biophys Mol Biol, 1996. **65**: p. 133–169.

Bouxsein, M.L., Boyd, S.K., Christiansen, B.A., Guldberg, R.E., Jepsen, K.J., Müller, R., *Guidelines for Assessment of Bone Microstructure in Rodents Using Micro–Computed Tomography*. Journal of Bone and Mineral Research, 2010. **25**: p. 1468-1486.

Brandi, M.L., Collin-Osdoby, P. *Vascular biology and the skeleton*. J Bone Miner Res, 2006. **21**: p. 183–192.

Britz, H.M., Jokihaara, J., Leppänen, O.V., Järvinen, T., Cooper, D.M., *3D visualization and quantification of rat cortical bone porosity using a desktop micro-CT system: a case study in the tibia*. Journal of Microscopy, 2010. **240**: p. 32-37

Brookes, M., Revell, W.J., *Blood supply of bone: scientific aspects*. London: Springer-Verlag, 1998. p. 108–41.

Buckwalter, J.A., Glimcher, M.J., *et al., Bone Biology*. Journal of Bone Joint Surgery, 1995. **77A**: pp. 1256-1289.

Buhl, K.M., Jacobs, C.R., Turner, R.T., *et al., Parallel changes in extracellular matrix protein gene expression, bone formation, and biomechanical properties of aging rat bone*. Journal of Musculoskeletal Research, 2002. **6**: p. 157-169.

Burstein, A.H., Reilly, D.T., Martens, M., *Aging of bone tissue: Mechanical properties*. J Bone Joint Surg, 1976. **58A**: p. 82-86.

Carter, D.R., Hayes, W.C., *The compressive behavior of bone as a two phase structure*. Journal of Bone and Joint Surgery, 1977. **59**: p. 954-962.

Cooper, D.M., Turinsky, A.L., Sensen, C.W., Hallgrímsson, B., *Quantitative 3D analysis of the canal network in cortical bone by microcomputed tomography*. Anat. Rec. B New Anat., 2003. **274**: p. 169–179.

Cooper, D.M., Thomas, C.D., Clement, J.G., Turinsky, A.L., Sensen, C.W., Hallgrímsson, B., *Age-dependent change in the 3D structure of cortical porosity at the human femoral midshaft*. Bone, 2007. **40**: p. 957–965.

Courtney, A.C., Wachtel, E.F., Myers, E.R., Hayes, W.C., *Effects of loading rate on strength of the proximal femur*, 1994. **55**: p. 53-58.

Currey, J., *Effects of differences in mineralization on the mechanical properties of bone*. Phil Trans R Soc Lond B, 1984. **304**: pp. 509-518.

Currey, J.D., *Strain rate and mineral content in fracture models of bone*. Journal of Orthopaedic Research, 1988. **6**: p. 32-38.

Currey, J., *The effect of porosity and mineral content on the Young's modulus of elasticity of compact bone*. J Biomech, 1988. **21**: pp. 13-16.

Currey, J., Brear, K., Zioupos, P., *The effect of ageing and changes in mineral content in degrading toughness of human femora*. J Biomech, 1996. **21**: pp. 79-84.

Diez-Perez, A., Gurri, R., *et al., Microindentation for In Vivo Measurement of Bone Tissue Mechanical Properties in Humans*. Journal of Bone and Mineral Research, 2010. **25**: p. 1877-1885.

Dilmanian, F.A., *Computed tomography with monochromatic x rays*. Am. J. Physiol. Imaging, 1992. **7**: p. 175–193.

Durbin, P. W., Williams, M.H., Jeung, N., Arnold, J.S., *Development of spontaneous mammary tumors over the life-span of the female Charles River (Sprague Dawley) rat: the influence of ovariectomy, thyroidectomy, and adrenalectomy-ovareictomy*, 1966. Cancer Res. **26**: pp. 400-411.

Fan, Z., Swadener, J.G., Rho, J.Y., *et al., Anisotropic properties of human tibial cortical bone as measured by nanoindentation*. Journal of Orthopaedic Research, 2002. **20**: pp. 806-810.

Feldkamp, L.A., Goldstein, S.A., Parfitt, A.M., Jesion, G., Kleerekoper, M., *The direct examination of three-dimensional bone architecture in vitro by computed tomography*. J. Bone Miner. Res., 1989. **4**: p. 3–11.

Feng, Z., Rho, J., et al., *Orientation and loading condition dependence of fracture toughness in cortical bone*. Mat. Sci. Eng. C – Bio, 2000. **11**: pp. 41-46.

Fratzl, P., Groschner, M., *et al., Mineral crystals in calcified tissues – A comparative study by SAXS*. J Bone Miner Res, 1992. **7**: pp. 329-334.

Fratzl, P., Weinkamer, R., *Nature's hierarchical materials*. Progress in Materials Science, 2007. **52**: pp. 1263-1334.

Gardner-Morse, M.G., Nelson, T., *et al., In Situ Microindentation for Determining Local Subchondral Bone Compressive Modulus*. Journal of Biomechanical Engineering-Transactions of the ASME. **132**.

Gerber, H.P., Vu, T.H., Ryan, A.M., Kowalski, J., Werb, Z., Ferrara, N., *VEGF couples hypertrophic cartilage remodeling, ossification and angiogenesis during endochondral bone formation*. Nat Med, 1999. **5**: p. 623–628.

Greenspan, F.S., Li, C.H., *Bioassay of hypophyseal growth hormone: The tibia test*. Endocrinology, 1949. 45: p. 455-463.

Hagaman, J.R., Ambrose, W.W., *et al., Age-related changes in rat trabecular, endosteal and cortical bone demonstrated with scanning electron microscopy*. Cells and Mater Suppl, 1991. **1**: p. 37-46.

Han, S.M., Szarzanowicz, T.E., Ziv, I., *Effect of ovariectomy and calcium deficiency on the ultrasound velocity, mineral density and strength in the rat femur*. Clin Biomech, 1998. **13**: p. 480–484.

Hansma, P.J., Turner, P.J., *et al., Bone diagnostic instrument*. Review of Scientific Instruments, 2006. **77**.

Hansma, P.J., Turner, P.J., *et al., The bone diagnostic instrument II: Indentation distance increase*. Review of Scientific Instruments, 2008. **79**.

Hansma, P.J., Yu, H., *et al., The tissue diagnostic instrument*. Review of Scientific Instruments, 2009. **80**.

Hildebrand, T., Laib, A., Müller, R., Dequeker, J., Rüegsegger, P., *Direct three-dimensional morphometric analysis of human cancellous bone: microstructural data fromspine, femur, iliac crest, and calcaneus*. J. Bone Miner. Res., 1999. **14**: p. 1167–1174.

Jamsa, T., Rho, J.Y., Zaifeng, F, MacKay, C.A., Marks, S.C., Tuukkanen, J., *Mechanical properties in long bones of rat osteoporotic mutations*. J Biomech, 2002. **35**: p. 161–165.

Jiang, Y., Zhao, J., Genant, H.K., Dequeker, J., Geusens, P., *Long-term changes in bone mineral and biomechanical properties of vertebrae and femur in aging, dietary calcium restricted, and/or estrogen-deprived/-replaced rats*. J Bone Miner Res, 1997. **12**: p. 820–831.

Johnson, W.M., Rapoff, A.J., *Microindentation in bone: Hardness variation with five independent variables*. Journal of Materials Science-Materials in Medicine, 2007. **18**: pp. 591-597.

Jowsey, J., *Variations in bone mineralization with age and disease*. In: Frost HM (ed) Bone biodynamics, 1964. P. 461-479.

Kannus, P., Järvinen, T.L., Sievänen, H., Kvist, M., Rauhaniemi, J., Maunu, V.M., Hurme, T., Jozsa, L., Järvinen, M., *Effects of immobilization, three forms of remobilization, and subsequent deconditioning on bone mineral content and density in rat femora*. J Bone Miner Res, 1996. **11**: p. 1339–1346.

Kiebzak, G.M., Smith, R., *et al., Bone status of senescent male rats: Chemical, morphometric, and mechanical analysis*. J Bone Min Res, 1988. **3**: p. 37-45.

Kirkeby, O.J., Berg-Larsen, T., *Regional blood flow and strontium-85 incorporation rate in the rat hindlimb skeleton*. J Orthop Res, 1991. **9**: p. 862–868.

Kotha, S.P., Guzelsu, N., *Tensile behavior of cortical bone: Dependence of organic matrix material properties on bone mineral content*. Journal of Biomechanics, 2007. **40**: pp. 36-45.

Kruzic, J.J., Kim, D.K., Koester, K.J., Ritchie, R.O., *Indentation techniques for evaluating the fracture toughness of biomaterials and hard tissues*. J. Mech. Behav. Biomed. Mater., 2009. 2: pp. 384-395.

Kuhn, J.L., Goldstein, S.A., *et al., Evaluation of a microcomputed tomography system to study trabecular bone structure*. J. Orthop. Res., 1990. **8**: p. 833–842.

Launey, M.E., Buehler, M.J., Ritchie, R.O., *On the mechanistic origins of toughness in bone*. Annual Review of Materials Research, 2010. **40**: pp. 25-53.

Lee, S., Davidson, C., *The tole of collagen in the elastic properties of calcified tissue*. J Biomech, 1977. **10**: pp. 473-486.

Leppanen, O., Sievanen, H., *et al., Three-point bending of rat femur in the mediolateral direction: Introduction and validation of a novel biomechanical testing protocol*. Journal of Bone and Mineral Research, 2006. **21**: pp. 1231-1237.

Li, X.J., Jee, W.S.S., *et al., Age-related-changes of cancellous and cortical bone histomorphometry in female Sprague-Dawley rats*. Cells and Materials, 1991. p. 25-35.

Lind, P.M., Lind, L., Larsson, S., Orberg, J., *Torsional testing and peripheral quantitative computed tomography in rat humerus*. Bone, 2001. **29**: p. 265-270.

Lucksanasombool, P., Higgs, W.A.J., Higgs, R., Swain, M.V., *Fracture toughness of bovine bone: influence of orientation and storage media*. Biomaterials, 2001. **22**: pp. 3127-3132.

Lundberg, R., Jenssen, B.M., *et al., Effects of short-term exposure to the DDT metabolite p,p0-DDE on bone tissue in male common frog (Rana temporaria)*. J. Toxicol. Environ. Health A, 2007. **70**: p. 614-619.

Margolis, D.S., Kim, D., *et al., Functionally improved bone in Calbindin-D28k knockout mice*. Bone, 2006. **39**: pp. 477-484.

Marotti, G., Zallone, A.Z., *Changes in the vascular network during the formation of Haversian systems*. Acta Anat (Basel), 1980. **106**: p. 84–100.

Marshall, G.W., Balooch, M., Gallagher, R.R., Gansky, S.A., Marshall, S.J., *Mechanical properties of the dentinoenamel junction: AFM studies of nanohardness, elastic modulus, and fracture*. Journal of Biomedical Materials Research, 2001. **54**: pp. 87-95.

Martin, R.B., Ishida, J., *The relative effects of collagen fiber orientation, porosity, density, and mineralization on bone strength*. J Biomech, 1989. **22**: pp. 419-426.

Matsumoto, T., Yoshino, M., *et al., Monochromatic synchrotron radiation muCT reveals disuse-mediated canal network rarefaction in cortical bone of growing rat tibiae*. J Appl Physiol, 2006. **100**: p. 274–280.

Matsumoto, T., Yoshino, M., *et al., Biphasic change and disuse-mediated regression of canal network structure in cortical bone of growing rats*. Bone, 2007. **41**: p. 239–246.

Matsumoto, T., Ando, N., *et al., Three-dimensional cortical bone microstructure in a rat model of hypoxia-induced growth retardation*. Calcif Tissue Int, 2010. **88**: p. 54-62.

Mazess, R.B., *Fracture risk: a role for compact bone*. Calcif Tissue Int, 1990. **47**: p. 191-193.

McCalden, R.W., McGeough, J.A., *et al., Age-related changes in the tensile properties of cortical bone: the relative importance of changes in porosity, mineralization and microstructure.*. J Bone Joint Surg, 1993. **75A**: p. 1193-1205.

McCreadie, B.R., Hollister, S.J., *et al., Osteocyte lacuna size and shape in women with and without osteoporotic fracture*. Journ. Biomech., 2004. **37**: p. 563-572.

McElhaney, J. H., *Dynamic response of bone and muscle tissue*. J Appl Physiol, 1966. **21**: p. 1231-1236.

McHugh, N.A., Haydee, M.V., *et al., In vivo rat assay: bone remodeling and steroid effects on juvenile bone by pQCT quantification in 7 days*. Am J Physiol Endocrinol Metab, 2003. **284**: p. 70-75.

Meyers, M.A., Chen, P.Y., *et al., Biological materials: Structure and mechanical properties*. Progress in Materials Science, 2008. **53**: pp. 1-206.

Mittra, E., Akella, S., Qin, Y.X., *The effects of embedding material, loading rate and magnitude, and penetration depth in nanoindentation of trabecular bone*. Journal of Biomedical Materials Research Part A, 2006. **79A**: pp. 1066-1072.

Morris, M., Finney, W., *et al., Bone tissue ultrastructural response to elastic deformation probed by Raman spectroscopy*. Faraday Discuss, 2004. **126**: pp. 159-168.

Mosley, J.R., March, B.M., Lynch, J., Lanyon, L.E., *Strain magnitude related changes in whole bone architecture in growing rats*. Bone, 1997. **20**: pp. 191-198.

Mow, V.C., Flatow, E.L., Foster, R.V., *Biomechanics*. Orthopaedic Basic Science, American Academy of Orthopaedic Surgeons, 1994. pp. 397-446.

Mullender, M.G., Van der Meer, D.D., *et al., Osteocyte Density Changes in Aging and Osteoporosis*. Bone, 1996a. **18**: p. 109–113.

Mullender, M.G., *et al., Ost eocyte Density and Hist omorphome tric Parameters in Cancellous Bone of the Proximal Femur in Five Mammalian Species*. Journ. Ortho. Res., 1996b. **14**: p. 972-979

Mullins, L.P., Bruzzi, M.S., McHugh, P.E., *Measurement of the microstructural fracture toughness of cortical bon using indentation fracture*. Journal of Biomechanics, 2007. **40**: pp. 3285-3288.

Nalla, R.K., Kruzic, J.J., *et al., Role of microstructure in the aging-related deterioration of the toughness of human cortical bone*. Materials Science and Engineering C-Biomimetic and Supramolecular Systems, 2006. **26**: pp. 1251-1260.

Norman, T. L., Nivargikar, V., Burr, D. B., *Resistance to crack growth in human cortical bone is greater in shear than in tension*. J. Biomech, 1996. **29**: pp. 1023-1031.

Nuzzo, S., Peyrin, F., *et al., Quantification of the degree of mineralization of bone in three dimensions using synchrotron radiation microtomography*. Med Phys, 2002. **29**: p. 2672–2681.

O'Brien, F.J., Taylor, D., Lee, T.C., *Microcrack accumulation at different intervals during fatigue testing in compact bone*. J. Biomech, 2003. **36**: pp. 973-980.

O'Brien, F.J., Taylor, D., Lee, T.C., *The effect of bone microstructure on the initiation and growth of microcracks*. J. Orthop. Res., 2005. **23**: pp. 475-480.

Parfitt, A.M., Mathews, C.H., *et al., Relationships between surface, volume, and thickness of iliac trabecular bone in aging and in osteoporosis. Implications for the microanatomic and cellular mechanisms of bone loss*. J. Clin. Invest., 1983. **72**: p. 1396–1409.

Pass, D., Freeth, G., *The rat*. ANZCCART News, 1993. **6**(4): pp. 1-4.

Pelker, R.R., Friedlaender, G.E., *et al., Effects of freezing and freeze-drying on the biomechanical properties of rat bone*. J Orthop Res, 1984. **1**: p. 405-411.

Peng, Z.Q., Vaananen, H.K., Zhang, H.X., Tuukkanen, J., *Long-term effect of ovariectomy on the mechanical properties and chemical composition of rat bone*. Bone, 1997. **20**: pp. 207-212.

Qiu, S., Schaffler, M. B., *Changes In Osteocytes, Lacunae and Canaliculi With Age in Osteons of Human Compact Bone*. Trans. 44th Annu. Meet. - Orthop. Res. Soc., 1998. p. 541.

Ramazan, K., *The effect of staining on the monotonic tensile mechanical properties of human cortical bone*. Journal of Anatomy, 2007. **211**: pp. 654-661.

Randall, C., Mathews, P., *et al., The bone disgnostic instrument III: Testing mouse femora*. Review of Scientific Instruments, 2009. **80**.

Rasoulian, R., *Characterization of swine femoral cortical bone using the reference point indentation technique*. MA thesis. University of Illinois at Urbana-Champaign, 2010.

Remaggi, F., Cane, V., *et al., Histomorphometric study on the osteocyte lacuna-canalicular network in animals of different species. I. Woven-fibered and parallel-fibered bones*. Ital J Anat Embryol, 1998. **103**: p. 145-155.

Ritchie, R.O., Kinney, J.H., Kruzic, J.J., Nalla, R.K., *Cortical Bone Fracture.* Wiley Encyclopedia of Biomedical Engineering, 2006. pp. 4152.

Roach, H.I., Mehta, G., et al., *Temporal Analysis of Rat Growth Plates: Cessation of Growth with Age Despite Presence of a Physis*. J Histochem Cytochem, 2003. **51**: p. 373-383.

Robertson, D.M., Robertson, D., Barrett, C.R., *Fracture toughness, critical crack length and plastic zone size in bone*. Journal of Biomechanics, 1978. **11**: p. 359-364.

Salem, G.J., Zernicke, R.F., *Diet-related changes in mechanical properties of rat vertebrae*. Am J Physiol, 1992. **262**: p. R318-R321.

Schneider, P., Stauber, M., *et al., Ultrastructural properties in cortical bone vary greatly in two inbred strains of mice as assessed by synchrotron light based micro- and nano-CT*. J. Bone Miner. Res., 2007. 22: p. 1557–1570.

Schoenle, E., Zapf, J., Humbel, R.E., Froesch, E.R., *Insulin-like growth factor I stimulates growth in hypophysectomized rats*. Nature, 1982. **296**: p. 252-253.

Sedlin, E. D.,Hirsch, C., *Factors affecting the determination of the physical properties of femoral cortical bone*. Acta Orthop Scand, 1966. **37**: p. 29-48.

Sissions, H.A., Kelman, G.J., *et al., A light and scanning electron microscopic study of osteocyte activity in calcium-deficient rats*, 1990. Calcif Tissue Int. **46**: p. 33-37.

Skedros, J.G., Hunt, K.J., *et al., Ontogenetic and regional morphologic variations in the turkey ulna diaphysis: Implications for functional adaptation of cortical bone*. Anat Rec Part A, 2003. **273**: p. 609-629.

Skedros, J.G., Hunt, K.J., *Does the degree of laminarity correlate with site-specific differences in collagen fibre orientation in primary bone? An evaluation in the turkey ulna diaphysis*. J Anant, 2004. **205**: p. 121-134.

Sone, T., Tamada, T., *et al., Analysis of three dimensional microarchitecture and degree of mineralization in bone metastases from prostate cancer using synchrotron microcomputed tomography*. Bone, 2004. **35**: p. 432–438.

Stauber, M., Muller, R., *Volumetric spatial decomposition of trabecular bone into rods and plates–a new method for local bone morphometry*. Bone, 2006. **38**: p. 475–484.

Stout, S.D., Brunsden, B.S., *et al., Computer-assisted 3D reconstruction of serial sections of cortical bone to determine the 3D structure of osteons*. Calcif Tissue Int, 1999. **65**: p. 280–284.

Swadener, J.G., Rho, J.Y., Pharr, G.M., *Effects of anisotropy on elastic moduli measured by nanoindentation in human tibial cortical bone*. Journal of Biomedical Materials Research, 2001. **57**: pp. 108-112.

Umemura, Y., Ishiko, T., *et al., Five jumps per day increase bone mass and breaking force in rats*. J Bone Miner Res, 1997. **12**: p. 1480–1485.

Vanleene, M., *et al., Relationships between density and Young's modulus with microporosity and physio-chemical properties of Wistar rat cortical bone from growth to senescence*. Medical Engineering and Physics, 2007. **30**: pp. 1049-1056

Vashishth, D., Verborgt, O., *et al*., *Decline in Osteocyte Lacunar Density in Human Cortical Bone Predicts the Accumulation of Microcracks With Age*. Bone, 2000a. **26**: p. 375–380.

Vashishth, D., Koontz, J., Fyhrie, D., *Age-Dependence of Osteocyte Lacunar Density Is Sexually Dimorphic in Human Vertebral Cancellous Bone*. Trans. 46th Annu. Meet. - Orthop. Res. Soc., 2000b. p. 702.

Vatsa, A., Breuls, R.G., *et al., Osteocyte morphology in fibula and calvaria-is there a role for mechanosensing?* Bone, 2008. **43**: p. 452-458.

Wachter, N.J., Augat, P., *et al., Prediction of cortical bone porosity in vitro by microcomputed tomography*. Calcif. Tissue Int., 2001. **68**: p. 38–42.

Walker, K. V. R., Kember, N. F., *Cell kinetics of growth cartilage in the rat tibia. II. Measurements during ageing*. Cell Tissue Kinet., 1972. **5**: p. 409–419.

Walsh, W.R., Guzelsu, N., *Compressive properties of cortical bone: mineral-organic bonding*. Biomaterials, 1994. **15**: p. 137-145.

Wang, X., Shen, X., *et al., Age-related changes in the collagen network and toughness of bone*. Bone, 1998. **31**: pp. 1-7.

Wang, X., Puram, S., *The toughness of cortical bone and its relationship with age*. Annals of Biomedical Engineering, 2004. **32**: pp. 123-135.

Whiteside, L.A., Simmons, D.J., Lesker, P.A., *Comparison of regional bone blood flow in areas with differing osteoblastic activity in the rabbit tibia*. Clin Orthop Relat Res, 1977. **124**: p. 267–270.

Yan, J.H., Clifton, K.B., Mecholsky, J.J., *Gower, L.A., Effect of temperature on the fracture toughness of compact bone*. Journal of Biomechanics, 2007. **40**: pp. 1641-1645.

Yan, J.H., Daga, A., Kumar, R., Mecholsky, J.J., *Fracture toughness and work of fracture of hydrated, dehydrated, and ashed bovine bone*. J Biomech, 2008. **41**: pp. 1929-1936.

Yeni, Y.N., Dong, X.N., Fyhrie, D.P., *et al., The dependence between the strength and stiffness of cancellous and cortical bone tissue for tension and compression: Extension of a unifying principle*. Bio-Medical Materials and Engineering, 2004. **14**: pp. 303-310.

Zioupos, P., *Ageing human bone: Factors affecting its biomechanical properties and the role of collagen*. J Biomater Appl, 2001. **15**: pp. 187-229.

Zwierzak, I., Baleani, M., Viceconti, M., *Microindentation on cortical human bone: effects of tissue condition and indentation location on hardness values*. Proceedings of the Institution of Mechanical Engineers Part H-Journal of Engineering in Medicine, 2009. **223**: pp. 913-918.